CERN/DRDC 94-49
RD-26 Status Report
21 Dec. 1994

STATUS REPORT OF THE CSI-RICH COLLABORATION/1994

DEVELOPMENT OF A LARGE AREA ADVANCED FAST RICH DETECTOR FOR PARTICLE IDENTIFICATION AT THE LHC OPERATED WITH HEAVY IONS

Bari Polytechnic/INFN, CERN, Coimbra University/LIP, Giessen Univ., Lausanne/EPF-L, Lund Univ., Munich TU, Padova Univ./INFN, Palaiseau/LPNHE- Ecole Polytech., Saclay/DAPNIA-SED, Sanita, INFN, Nantes/SUBATECH, Rehovot/Weizmann Inst., Zagreb/ R. Boskovic Inst.

Spokesmen: G. Paic, F. Piuz

A. di Mauro, L.M. Galantucci, A. Grimaldi, E. Nappi, F. Posa, T. Scognetti, A. Valentini, V. Valentino
INFN Sez. Bari and Politecnico, Bari, Italy

A. Braem, F. Piuz, J.C. Santiard, J. Schukraft, S. Sgobba, T.D. Williams
CERN, Geneva, Switzerland

R. Ferreira-Marques, A. Policarpo
L.I.P., University of Coimbra, Coimbra, Portugal

W. Hejny, W. Kuehn, R. Novotny, S. Riess
University of Giessen, Germany

J. Almeida, H. Berger, C. Coluzza, G. Margaritondo, T. dell'Orto
E. P. F. -Lausanne, Switzerland

H.A. Gustafsson, A. Oskarsson, O. Svensson
University of Lund, Sweden

J. Friese, P. Maier Komor, A. Gillitzer, J. Homolka, K. Zeitelhack
Technical University Munich, Germany

R. Martinelli, L. Peruzzo, P. Sartori, G. Sartori
INFN Sez. Padova, Italy

Ph. Miné, G. Vassileiadis
Palaiseau, LPNHE, Ecole Polytechnique, France

P. Besson, Ph. Bourgeois
Saclay, DAPNIA/SED, France

F. Garibaldi
INFN sez. Sànita, Roma, Italy

G. Paic *)
SUBATECH, Nantes, France

A. Breskin, A. Buzulutskov, R. Chechik
The Weizmann Institute of Science, Rehovot, Israel

A. Ljubicic Jr., T. Tustonic.
R. Boskovic Institute, Zagreb, Croatia

*) on leave of absence from R. Boskovic Institute,Zagreb, Croatia.

1- Introduction.

A RICH detector for Heavy ion collisions at LHC using a CsI photocathode (PC) has to demonstrate the capacity to efficiently detect and identify particles in a high density environment of up to 8000 particles per rapidity unit.
To achieve that task there are several requirements that have to be met:
-a density of photoelectrons around the ring perimeter that is much larger than the surrounding noise, implying a quantum efficiency (QE) of photoelectric conversion of a satisfactory value,
-a stability in time compatible with the duration of the experiment,
-a pattern recognition method that can successfully identify the Cherenkov angle using the impact point of the charged particle measured in the detector itself, the momentum, and angle of incidence measured by the tracking detectors inside the ALICE barrel,
-a judicious engineering design of the barrel modules including a radiator of suitable transparency,
-a frontend electronics capable of detecting with high efficiency the UV induced photo electrons created by the photons, at the interaction rates expected at the LHC in the heavy ion mode (10E4).
All these considerations were taken as our milestones for the 1994 programme.

A major part of our effort has been devoted to the improvement of the photoconversion efficiency of our large photocathodes. Renewed efforts have been prompted by the results of the groups in the collaboration evaluating the CsI QE by means of UV sources on small samples. They have discovered that a large part of the persisting disagreement in the QE values were due to a large extent to wrong photon flux measurements caused by erroneous calibrations given by manufacturers of photomultiplier tubes.

The consequences of this observation was twofold. The measured QE within different groups of RD26 became consistent among themselves and much closer to the high values measured by several other groups (Seguinot, [1] Anderson, [2]). The value of QE measured in 1993 using Cherenkov photons in a RICH prototype [3,4], that were compatible with the old UV light measurements, became concurrently 50% lower than the new corrected ones. This development forced us to reconsider our results obtained with those large photocathodes and explain why were the RICH results so much different from the QE measured on small samples.

To that purpose we have started systematic studies of our CsI deposits using a large number of methods. As will be demonstrated the results of these analysis have indicated the importance of the substrate for the PC operation. As a result several new substrates technologically compatible with large area photocathodes have been produced and tested in beam. We review the main results obtained on the surface measurements, the development of the new substrates, the very encouraging results obtained with a 30x30cm2 prototype in a pion beam, compatible with UV laboratory tests. For the first time, a proof of principle of the operation of a large CsI PC in a fast RICH has been obtained close to its optimum performance.

The design of the ALICE RICH barrel structure was started, allowing to define more accurately the constituting modules. In particular, emphasis was put on the development of a large liquid radiator array providing hints on a realistic segmentation of the detector.

The simulation group incorporated the new results as realistic inputs to their programmes. The pattern recognition algorithms were tested using our latest raw Cherenkov patterns from the test beam, randomly superimposed in order to achieve a 50 part./m2/ event density: a pi/K 3 sigma separation up to 2.6 GeV/c was achieved at that particle density. A realistic RICH barrel design was implemented into the ALICE GEANT simulation.

We report also on the development of the frontend pad electronics - specifically on the first tests of the Gassiplex chip.

2- Laboratory investigations of the quantum efficiency of CsI.

The photoemission properties of CsI layers were intensively investigated in several cooperating laboratories. Evaporations and substrates were either prepared at every laboratory or exchanged betwen them for cross checking.

2-1 QE in vacuum, general

At the Weizmann Institue, the QE in vacuum was investigated with a monochromator system attached to a CsI evaporation chamber. Samples on various substrate materials were investigated in situ namely without breaking the high vacuum (10-7 Torr) following the evaporation. The best results, on all tested materials (polished stainless steel, silicon, Cu/Au, Ni and Ni/Au on printed boards) were obtained when evaporating on a substrate kept at 60°C. Right after evaporation, the samples have a low quantum QE , which considerably increases in vacuum, under 60°C within a few hours, as shown in fig. 1. The QE, normalized to a photomultiplier tube calibrated against a NIST vacuum photodiode [5] has been well reproduced (within 10%) over several tens of samples produced.

At Munich, Palaiseau and Saclay, evaporation and measurement facilities were separated, implying a short exposure to air or gas during the transfer from one device to another. Phototube calibrations were also different at Munich and Saclay. Observations were found concording and in good agreements between labs allowing to define a QE curve taken as a reference curve for RD-26. The significantly higher result found in Munich was not included in that reference and still demands further investigations. These results are shown in fig. 2.

2-2 The role of the gas and the electric field.

The Weizmann group has demonstrated in extensive laboratory measurements, and in parallel, measurements at CERN with a RICH detector confirmed (section 4), that the UV-detector gas plays an important role in the photoemission properties of CsI [6,7]. Measurements were carried out at high electric fields (in a gas multiplication mode) and at very low electric fields at the PC surface (in collection mode). The relevant parameter is in fact the E/p value.

The measurements at the laboratory were made in various hydrocarbon gases: CH4, C2H6, i-C4H10 and in gas mixtures: CH4/i-C4H10, He/CH4, and He/i-C4H10, in the pressure range 0.05-1 atm. Concurrently, the photoelectric yield of large CsI PCs was measured in a RICH detector equipped with a MWPC operated at atmospheric pressure with similar gas mixtures (section 4).

We confirm that the photoelectron extraction from solid PCs into gas media has a universal behaviour as a function of the field. In a charge collection mode, the QE value is lower than that in vacuum and is independent of the field. In a charge multiplication mode, the QE increases with the field and reaches the vacuum value at high gas gain. Translated into detector practice, high field values are obtained at the PC surface in a parallel plate chamber at low pressure and low field values in a MWPC operated at atmospheric pressure.

The most pronounced behaviour, leading to very large difference in the QE as a function of E/p, has been observed for the He-based gas mixtures (Fig. 3-a) where a reduction factor of 2.5 has been observed. On the other hand, in pure CH4 and CH4/hydrocarbon mixtures the QE is practically independent of E/p and is close to that in vacuum even at low fields and at atmospheric pressure (fig. 3-b). These results are of prime importance for the selection of gas mixtures in large MWPC operated with a CsI PC. That discussion will be continued in the RICH section.

The difference in photoemission (at low E/p) between various gases is explained by the different probability for the photoelectron elastic backscattering. This phenomenon is presently under theoretical investigations.

2-3 QE enhancement at very high electrical fields.

We have demonstrated that under very high electric fields the QE of CsI is enhanced in a considerable way. Fig.4 shows the relative field-enhancement of the CsI at three wave lengths, as measured with a thin wire PC. In such a setup, field up to 500 kV/cm were reached. The QE enhancements vary from 1.5 to 25 over the respective wavelength range of 160 to > 200 nm [8]. It is interpreted as being due to a decrease in electron affinity at very high electrical fields. That phenomenon could be exploited in practice, provided we find ways to create high electrical fields at the PC surface [9], which is the subject of intensive investigations.

2-4 The role of the substrate material.

The best QE results were obtained so far on polished stainless steel substrates. The QE of CsI PCs measured in the laboratory made on Cu/Au layers on G10 plates, forming the pad electrodes of RICH detectors, was in general 30% or more inferior to that of RD26 reference. Recent surface studies with various microanalysis techniques [10] revealed that CsI layers deposited on such substates have a very inhomogeneous morphology. The QE of new substrates (see section 3), made of G10-coated nickel and showing a better surface structure, were found about 10-15% lower than the reference. It was demonstrated that an exposure to air of 15-30 min. (rel. humidity below 50%) has a very small effect on the QE.

As seen in fig. 2, the Saclay group measured QE values in agreement with the RD26 reference on aluminized mylar or nickel coating. They observed a decrease by a factor of 2 on pure copper substrates.

2-5 Angular incidence effect.

In most RICH applications and in particular in the proximity-focusing geometry, the UV-photons impinge on the CsI surface under large angles (40-60°). We found it important to measure the QE dependence on the angle of incidence since the reflection loss significantly depends on the polarization state of the photon in case of a dielectric surface. This effect was measured with CsI deposited on conical surfaces [11] in vacuum. As shown in fig 5, we found that there is a monotonic decrease of the QE with wavelength, reaching 30% at 210 nm under an incidence angle of 55°, compared to normal incidence. This effect is attributed to possible surface irregularities which could affect the photemission (see section 3). Further investigations are requested to clarify this angular effect.

2-6 Theoretical modelling of the photoemission

The Weizmann group investigated theoretically the UV-induced photoemission properties of CsI. We have developed a microscopic model treating radiation-induced photoemission from alkali halides, based on first principles [12]. The model starts from the primary interaction of photons with the photocathode and follows the low-energy electron transport in the solid. In the eV range, this transport is principally guided by electron-phonon interactions.

Using this model, we could reproduce in a remarkable way the QE of CsI, both in the transmission and reflection modes. The results are shown in fig 6. The model also accurately predicts the electron escape length from CsI and the average photoelectron energy. We intend to compare the model predictions to the secondary electron spectra obtained with the Electron Spectroscopy for Chemical Analysis (ESCA).

Other models were developed to describe the QE-dependence on the electric field, at high electric fields (see above) [8].

3- Microanalysis of the CsI layers.

A large scale study has been undertaken by groups at CERN, EPF-L, and Weizmann on the various aspects of the surface structure, of the chemical composition, of the CsI layers and finally of the photoemission properties.

The studies were made with a number of complementary methods. Morphological information, given by the scanning electron and tunneling microscopes (SEM and STM), was compared to the 2-D imaging of the primary or secondary electron emission at a similar lateral resolution (micron range). The latter were obtained with the laterally resolved electron microscopy for chemical analysis (ESCA), the photoemission electron microscopy (PEEM) and the atomic force microscopy (AFM). Structural information were also obtained from X-ray diffraction measurements. We limit ourselves to the main findings of these studies. The extensive report on the measurements and results will be published in [13].

3-1 The old substrates

The CsI layers evaporated on "high quality" substrates like polished stainless steel, aluminium, glass or silicon are characterized by a structure composed of contiguous microcrystals with dimensions ranging from .3 to 3 µm. The CsI deposits on "rough" substrates such as printed circuit boards (G10 with copper covered with a thin layer of chemical gold) that were used in our tests of RICH detectors so far, exhibit a very non-homogeneous texture as shown on fig. 7-a. Measurements of the secondary emission have confirmed that close to half of the surface was completely inactive i.e. did not emit photoelectrons as seen in fig. 8-c.

On top of that a particular phenomenon was observed - namely the X-ray diffraction spectra of CsI evaporated on pure Cu substrates and on gold covered copper exhibited preferentially peaks of pure Cs and pure Iodine instead of peaks belonging to CsI. Many observations were made showing evidences of Cs/I segregation over a large range of distances with the STM, the ESCA (fig. 9) and also by X-ray diffraction. We surmise that Cu promotes during evaporation the dissociation of the CsI or prevents its formation from the vapor phase.

3-2 New substrates.

Following the findings described above, we set to produce a highly polished board with a dense layer covering the copper one which is necessary for pad etching purposes. We decided to keep the standard etching process because it is accessible in price for large areas and compatible with the technical requirements to the operation of a multi wire proportional chamber (MWPC) such as the manufacture of large pannels with electronics connections . The following procedure was adopted:
- production of the pad printed board on G10 and copper only, using standard etching technique,
- alumina paste and chemical polishing of the copper,
- chemical deposition of a thick homogeneous nickel layer (15 μm); a thinner gold layer was also added on some PCs,
- molten tin was also tried but with poor results at the level of the overall quality of the circuit.

The results of the beam tests of these PC's will be reported later in this report. Here we want to point out that PC's made on these substrates have demonstrated surface qualities that are at the level of the best ones made on polished substrates used to measure the quantum efficiency on small samples. On the structure revealed by the SEM (Fig. 7-b,c) and the PEEM measurements made in the VUV region (fig 8-a,b), we observe a tremendous difference with respect to the surface structure of the previous PC shown in Fig 7-a and 8-c respectively. The structure of the CsI layer is identical to the one seen on the good quality substrates (stainless steel, silicon and like)

The X-ray diffraction spectra show clearly identified CsI peaks and no pure Cs peaks. However after several hours at the atmosphere some segregation of CsI is observed in the X-ray diffraction spectra. The evolution of this process seems to be very slow, confirmed also by the results of the beam tests and laboratory measurements after exposure to air; after periods of exposure of the order of 30 min, no appreciable loss in QE was observed.

The heat treatment at temperatures of ≈ 55°C under vacuum after evaporation has been demonstrated by several groups within RD26 to have a beneficial influence on the QE with no incidence on the surface topography. Indeed the ESCA measurements [4] have demonstrated a change in the shape of the 3d lines belonging to Cs and I as well as a change in the shape of the secondary emission spectrum. However when the heating is increased to 70 ° the morphology of the surface changes and the QE decreases. As yet, no attempt has been made to determine more precisely where the critical temperature for the deterioration lies.

In conclusion we may say that using the above methods we have succeeded in obtaining a better understanding of the influence of the substrate on the CsI layer topography and secondary electron emission, allowing us to determine several substrates technologically feasible for large size detectors. Several new physical observations will allow to progress in the understanding of the ageing process of CsI layers and will provide methods for controlling the production of large layers. These studies, taken in charge by specialized and well equipped groups, are of crucial importance to ensure reproducibility and long term operation of CsI PCs.

3-3 New materials.

Two new materials have been tested for photoconversion in the UV range by the Ecole Polytechnique Palaiseau. Both materials are solids and were deposited in the same way as CsI. One of them the Bis(cyclopentadin)Magnesium gave no measurable signal at any wavelength while the other one - TetraThiaFulvalenium-TTF gave a low response in the range of UV photons between 140 and 220 nm at the level of .5% percent at the lowest wavelength and .001% at 220nm.

4- Fast RICH and CsI photocathodes.

The aim of our tests is twofold. We first have to evaluate the QE of our PCs in the environment of a fast RICH detector, with single Cherenkov photons emitted at large incident angles on CsI layers deposited on large printed board substrates. Secondly, we have to characterize the detector in terms of number of photoelectrons detected per ring, leading to evaluate essentially the UV transmissions of the components - radiator, window, gases, grid- and the detection efficiency of single electrons by the MWPC.

4-1 Evaluating the CsI QE from fast RICH measurements

The schematic of the fast RICHs used is shown in fig. 10. The CsI layer is deposited on the cathode of a MWPC, segmented into pads of size 8x8mm2. The MWPC, detecting the single electrons emitted from the CsI layer, has a distance anode-cathodes of 2 mm and sense wires of 20 μm diameter spaced by 4 mm. The second cathode, made of wires or of mesh, defines the active volume of the MWPC. The proximity gap extends up to the radiator to provide the distance necessary for achieving sizeable Cherenkov ring radii. The entire volume is flushed with a UV transparent gas, typically methane. A third wire electrode, positively polarized, is located close to the radiator with the purpose of collecting the electrons created by the particles traversing the wide proximity gap [3].

We remind the main features of our method. One has the basic relations:

number of photons= $N_{ph} = 370.\ L.\ Tr_{grid} \int QE.\ Tr_{rad}.\ Tr_{qu}.\ Tr_{gas}.\ Ref.\ \sin^2\theta.\ dE$ (1)

number of detected electrons= $N_{el} = \varepsilon_{det}.\ N_{ph}$

with the refractive index of the radiator n= n(λ) and $\cos\theta = 1/\beta.n$. All transparencies (Tr) and reflections (Ref) are measured in the ΔE (Δλ) range of interest.

As shown last year [3], the dependence of QE on λ can be directly measured with a highly chromatic radiating medium, like NaF, by counting the photoelectrons spread into circular zones of widths equivalent to a small enough dλ. The radiator in use this year, liquid C6F14 of low chromaticity, was chosen for its better Cherenkov angular resolution and a UV transparency easy to monitor. Since the low chromaticity hinders a direct differential QE measurement, the QE curve will be obtained from (1) by simulation calculations. Hence the QE shapes are not under full experimental control and the method is more appropriate for an evaluation of the integrated QE. That point will be discussed later on from the results.

The method is based on the counting the number of photoelectrons per ring. As described in [3], the localization of the single electrons is achieved by measuring the spread of the induction of the avalanche on pads using an analog electronics. To every single electron will be associated a "pad cluster" the mean size of which is typically 1.6 to 2.1 pads depending on the chamber amplification. A ring will appear as a pad pattern. Depending on the ring radius and the number of photoelectrons, pad overlapping will result from the sizeable pad area in use (8x8mm2). Fig. 11 shows the overlap fraction, in term of number of photon per pad cluster, at various photon densities and ring radii.

Two methods are used to disentangle the pad pattern in terms of individual photons: i) a pad cluster finding analysis, efficient in case of a few photons per ring but limited in case of large cluster size because of an increasing overlap probability, ii) division of the total pad pulse height measured in a fiducial zone by the mean pulse height of a single electron. The single electron pulse height distribution, expected of exponential shape, is extracted from a selection of well separated single electron clusters (see fig. 20-a). To achieve that, we measured events with only a few photoelectrons per ring reducing the thickness of the radiator.

In what follows, the experimental results are compared to a simulated pad pattern generation where:

- Cherenkov photons are generated in a C6F14 radiator acccording to its thickness and the particle velocity,
- photon losses are calculated from known UV transparencies and reflectivities of the detector components
- photoelectrons are generated from known impacts at the pad plane using a given CsI QE curve
- a pad pattern is generated for every single electron using the known spread of induction and an exponential pulse height generator of fixed mean (SEPH)
- single electron pad patterns are overlapped and compared to a threshold providing the necessary information per ring: total pad pulse height (TPPH), number of pads hit/ring, number of pad clusters, cluster size, etc...

4-2 Results of the tests

Our tests were carried using two fast RICH prototypes. The first one has a cathode size of 96x256 mm2, allowing for ring radii of 40 mm. The second one, of size 288x320 mm2, allows to study rings of radii varying between 35 to 120 mm radius, thanks to an in situ adjustement of the distance radiator to pad plane. The thickness of the liquid C6F14 radiator can also be varied from 0 to 15 mm. The C6F14 is circulated through an oxysorb purifier and a cell for UV transparency measurements.
The small RICH was used for testing a series of CsI pad cathodes for the sake of economy. The front end electronics provides a multiplexed analogue measurement of every pad signal [14].

The RICHs were tested at the PS/T11 line, using pion/proton at 3 GeV/c. The event selection was provided by a 4-fold scintillator coincidence defining a beam size of about 1 cm2 at the middle of the pad cathode.

After the convergence of the CsI QE beam measurements with UVUV monochromator tests towards higher values, it appeared that our results obtained last year from 10 large PCs were achieving about 30-50% of that new reference QE value.To be reminded in 1993, the CsI evaporations were done on standard printed boards (SPB), composed of G10, copper and chemical gold with no special polishing. In addition, they were all done on the same pad plane after removing the previous CsI layer.

4-2-1 CsI QE measurements on new pad substrates

Four small PCs (PC15,16,17,18) and one large (PC19) were produced using the new substrates described in section 3: PC15, 16, 17 had only a nickel layer, PC18, 19 had the additionnal gold layer. The polishing procedure was optimized from PC17 onwards. The next operations in the production of PC15 to 18 were:
- assembly of the pad electrodes with frame and connectors,

- outgassing of the electrode at 50 °C
- outgassing in the evaporation station at 40 °C for one day
- CsI evaporation on hot substrate (40°C, 1-3 10E-6 torr)
- electrode kept after evaporation under vacuum at the same temperature (1hour)
- introduction of argon in the vacuum vessel.

Only PC19 was heated at 50°C and kept 12 hours in the vacuum station after evaporation.
The mounting of the PCs on the detector in presence/or not of air is discussed in the section 4-2-4.

A detailed series of test results is presented for PC17 and PC19. Measurements were taken at different radiator thicknesses and different voltages. The chamber gas was methane and the particle momentum 3 GeV/c.

Several single events pad patterns are displayed in fig. 12 showing the central cluster of the particle surrounded by the single electron clusters.

In fig 13-a,b, the mean number of pads, of photoelectrons obtained as the ratio TPPH/SEPH and of pad cluster per ring is compared to the simulation for PC17 and PC19. It can be seen that:
- a good fit is obtained for the number of photoelectrons while the number of pads and of clusters is overevaluated by the simulation. It implies that the ratio photon/cluster, shown in fig 11, is found larger in the data by about 10-20%. It could be that the spread of induction used in the simulation is too large, noticing that the measurement and simulation of the number of photoelectrons is independent of that shape which relies essentially on the correct determination of the TPPH and SEPH.
- a larger number of photoelectrons/unit length is found at small radiator thickness, due to an increase of the UV transmission at low wavelengths where the QE is the highest.

These observations provide insights in view of the optimization of the number of photons per ring (or radiator thickness), pad size and ring radius to be selected in order to get a ratio photon/cluster close to unity and a performing identification.

In fig. 14, we compare to the RD26 reference the two extreme QE curves used in the simulation to fit the data. The best result was obtained with PC19, the four other results varying between the 2 curves. Although using that arbitrary procedure, a simple scaling of the reference curve was found insufficient for fitting data over the whole radiator thickness range: the QE values at high wavelength had to be more attenuated than those at low wavelength. That feature is in agreement with the fact that the surface structure effects seem to be the most pronounced at large wavelengths.

The hatched area in fig. 14 corresponds to the QE measurements obtained last year with the copper/gold substrates [3,4]. Although these measurements were taken at different radiator transparencies (NaF), quantity under close control only in our last set of measurements, they were reproducible enough to attribute the improvement observed on the 5 last PCs to the new substrate technology adopted.

4-2-2 Evaluation of the photon feedback

Some of the UV-photons emitted by an avalanche are converted into electrons at the CsI surface. That photon feedback mechanism is a source of background and may initiate discharges at a too high gas amplification.

We first evaluated that contribution by measuring without radiator the photons emitted by the particle avalanche in absence of Cherenkov photons. Their radial distribution is found compatible with the emission from a point source. Only 30% of the events are correlated with the emission of one photon. Their PH contribution was evaluated in the Cherenkov fiducial zone to be substracted from TPPH measurements.

In case of Cherenkov events, the low level of the overall photon feedback contribution is seen in fig. 15-a showing the angular distribution of emission of single photons in the whole angular range, including the particle and the photoelectrons.

Measurements were taken at different voltages in order to confirm the low level of photon feedback and the validity of the determination of the number of Cherenkov photoelectron by measuring the TPPH. As seen in fig. 16, there is still a good fit to the data, indicating that there is no need of an extra source of photons (feedback) to correctly simulate the TPPH up to our highest gas amplification (≈ 1. 10E 5).

These measurements are of prime importance since they indicate that a large CsI PC can be operated in a fully open geometry filled with methane, free of any "box or cloison" structures, with a negligible amount of photon feedback. In addition, we observed a very stable operation of our MWPCs during two years (20 PCs) characterized by an immediate HV conditioning and an absence of discharges or breakdown under irradiation.

These features are related to our low gain operation, 0.5-1.0 10E5, made possible due to the use of a frontend amplifier of long integrating time, 400 ns. Other experimentalists [15], have experienced instabilities when using time constants as short as 30 ns requiring higher gain operation to achieve satisfactory detection efficiency. Such a long time constant is of no consequence at ALICE, thanks to the low event rate expected in the ion collision mode. That may not be the case in other applications such as pp/LHC. More effort has to be put on that problem by looking at efficient quenchers and optimized electronics in order to preserve the simplicity of the layout. A programme is undertaken at RD26 investigating the photon feedback threshold in different gas mixtures (see section 4-2-5).

4-2-3 Fast RICH performance: number of photoelectrons, Cherenkov resolution.

With the CsI QE achieved on PC19, a mean of 14 photoelectrons per ring of 100 mm radius (3.0 GeV/c pion) were obtained from a C6F14 radiator of 10 mm thickness. Out of these 14 electrons, 10 can be identified as well separated pad clusters. This result was achieved with a MWPC cathode made of a mesh of poor transparency, 74% at 52° photon incidence. Using a wired cathode of 95 % transparency (100 μm wires spaced by 2mm) a straightforward increase of 20% may be achieved. An additional 5% gain is expected from the new more sensitive pad electronics. (section 7). Finally, 16-18 photo electrons per ring can be expected with the CsI QE as achieved in PC19.

A similar small RICH is now under test by the Saclay group at SATURNE. The best result obtained on old substrates is about 8 photoelectrons per ring at $\beta=1$ with a sealed C6F14 radiator of 10 mm thickness.

A larger RICH, of size 50X50 cm2, is under completion in Munich and will be tested early next year.

Figs. 15 and 17 show some Cherenkov angle distributions measured in the large RICH. They were calculated with/without fiducial cuts, taking the photoelectron localizations either from the centres of any hit pad or from an analog centroid calculation for clusters of 2 or more pads. The low fraction of hits that does not belong to a ring is apparent in the distributions where no fiducial cuts are applied (fig 15-a). Improving the localization accuracy using the centroids improves the angular resolution from 10 to 8 mrad per photon (fig 17-a,b).

In fig. 18, the Cherenkov radii measured in the small and large RICH for different radiator thicknesses are compared to the simulation, showing excellent agreement.

4-2-4 Influence of air exposure, ageing evaluation

When measuring the QE of small samples the evaporation of the CsI layer, the heating treatments and the UV measurements are done without breaking the vacuum. That is not the case for large PCs where an exposure to air (10-20 min) occurs at the transfer of the PC from the vacuum vessel to the detector. To determine the influence of such an exposure, two small PCs (PC16 and 17) were protected by a tight box in the vacuum vessel and filled with argon. The mounting on the detector was also performed in a glove box filled with argon, without any exposure to air. The PCs were measured at the beam. After that reference measurement, the PCs were exposed twice to air at the beam zone, for 15 and 30 minutes. The two measurements after these exposures were found identical to the reference one. From these tests, we learned that i) efforts for further QE improvements should regard the basic processing, the contact with air making no harm to the PC, ii) the mounting of large PCs can be done in air, avoiding cumbersome manipulations in a glove box, iii) CsI PC's have some immunity to air so that their preservation over large periods of time is conceivable without extreme precautions and could even support short exposures to air.

However, our tests were performed over short time periods (1-2 weeks). We should confirm these results over longer periods since it is still possible that a slow reaction could have been initiated during the exposure provoking a delayed deterioration.

One large PC (PC13 of low QE) was measured 3 times at the beam over a 5 months period, keeping within experimental fluctuations a constant photoelectron yield. That PC was kept under methane or argon flow.

At Saclay, two small PCs were kept under methane flow during three and six months respectively. Their QEs were monitored with a UV lamp. As seen in fig. 19, after an increase of the QE during the first days following the evaporation, the QE value stays stable and no clear degradation was observed.

4-2-5 Test of new gas mixtures

All our tests were performed with methane or methane/i-C4H10 (95/5) which have good UV transmission and quenching properties. However, in such a large array as proposed at ALICE, any reduction of the flammable gas volume is welcome. To that purpose, we have tested the following mixtures: A/CH4 (50/50), (80/20), A/CH4/i-C4H10 (86/7/7), A/i-C4H10(80/20) and He/i-C4H10 (90/10), referred as M1 to M5 respectively.

A first analysis has shown that the photo electric yield of the CsI PC is not affected when using argon based mixtures but a 40% loss is observed in the M5 mixture with helium. The latter was also found with the UV lamp at Weizmann with a more pronounced loss (100%). As described in section 2, that effect is attributed to electron backscattering in a noble gas at low E/p. For comparison to the Weizmann results, our E/p value was 2.0. It is quite interesting that the photoemission yield of CsI is preserved in argon (not yet measured at Weizmann).

A photoemission line at 120 nm from avalanches in argon is expected to enhance the photon feedback level. As shown in fig. 15-b, such an increase, by a factor of 2 to 3, is observed in M2 and the admixture of a better quencher (i-C4H10) restores the low photon feedback as seen in M3 and M4. Also, the distribution of the single electron PH spectrum is no more purely exponential as observed in methane, reflecting the well known photonic activity in avalanches in noble gases (fig. 20-b).

These first results open the perspective of reducing by large factors (4-5) the volume of flammable gas in a large detector. These studies are pursued in the laboratory investigating more efficient and UV transparent quenchers like neopentane.

5- Pattern recognition and simulation.

5-1 Evaluation of the RICH performance for ALICE

The density of particles reaching the ALICE RICH would be of the order of 50 particles/m2 at 3.6 m from the collision point. We wanted to evaluate the performance of our current prototype in high multiplicity collisions.
To achieve this we used an "imaginary" 48 X 48 cm2 (60 X 60 pads) RICH detector in which we uniformly overlapped the events obtained from the actual 32.0 X 28.8 cm2 RICH prototype (PC19 in section 4). The overlap was done by translating the single-ring prototype image in x- and y-coordinate randomly over the area of the larger imaginary detector and simply superimposing (adding) the raw pad data and thus creating an image that corresponds to a high-density event. Four sample images thus obtained are shown in Figure 21. It is important to note that no selection was made on the single events except that we artificially increased the proton/pion ratio using the TOF information from the test-beam setup.

The detector parameters chosen correspond to the ones used in previous Monte-Carlo studies [16,17] : 1.0 cm freon thickness and 7.0 cm proximity gap width. The momentum used was 3.0 GeV/c which will give a higher density of actual pads due to the fact that some particles in ALICE conditions will not generate rings (because they are below the Cherenkov threshold) and that the momentum distribution of pions at the ALICE-RICH is peaked at low values (~350 MeV/c) thus generating rings with smaller radia and smaller number of photons per ring. To correct for this we used only 10 particles in the 48 X 48 cm2 area which would correspond to ~44 particles/m2 but gives a similar pad occupancy as the 50 particles/m2 ALICE event.

To evaluate the performance of the method used to analyse high-density data [17] we first analysed single-ring runs. The coordinates of the impact point were determined from the center-of-gravity of the MIP ionization pattern on the pad chamber. This was necessary because our experimental setup allowed uncertainties in the beam position of the order of ± 4 mm. We think that such a precision would be comparable with realistic conditions at the ALICE experiment and with the precision of the tracking detectors in the ALICE setup. A check on the impact angle showed that our prototype was inclined 1.0 ± 0.1 degrees relative to the beam axis so this angle was used for the analysis.

The results are shown in Fig. 22-a together with a gaussian fit to the pion distribution. The three-sigma pion/kaon separation obtained would correspond to 3.3 GeV/c particles. Note that the results are remarkably clean since there was no previous selection of events. We analysed everything that was on tape including possible interactions in the detector volume, events with an ionizing particle passing across our detection volume, events which are noisy due to pedestal problems, events with a small photon number etc. We hope that such an indiscriminate approach makes our analysis more realistic.

The results of the same procedure applied to the superimposed events are given in Figure 22-b. The results shown include only particles that fell more than 10 cm away from the detector edges since the edge effects should be studied more carefully. Note again that the results are very clean since we did not apply any cuts in the raw data thus the detector+analysis efficiency is 100% in the fiducial area in the center of the detector (10 cm away from the edges). The RMS is 7.0 mrad which corresponds to a kaon/pion three-sigma separation at 2.6 GeV/c.

The Monte-Carlo simulation for which the same generation and analysis procedure is applied with the same density gives values of 5.6 mrad for the RMS of the pion angle. The difference is still under study but it can be attributed to an unknown spread in the incident angle of our present setup and to the small percentage of raw events which involve interactions in our detector volume and other noisy raw events for which no attempt was made to remove them from the raw data sample used.

5-2 GEANT simulation

The engineering design for the RICH as proposed in the present report has been integrated in the ALICE simulation package GALICE. So far only several SHAKER (the ALICE event generator) events have been used to check the methods. Due to computing limitations caused by the multiplicity of events (8000 per rapidity unit), we have so far made preliminary calculations only for the central ring of modules located at rapidity zero. The particles (primaries as well as secondaries formed in the detectors laying in between the vertex and the RICH) and the secondary particles created in the RICH itself are known by species, charge, momentum and incidence angle.

With a multiplicity of 8000 produced particles/unit of rapidity the number of particles reaching the RICH central wheel(i.e. one of the 5 wheels constituting the ALICE RICH barrel) which has a total area of 30m2 is 1780 of which 338 will be lost in the frames for a total efficiency of 78%. The particle density is 59 particles /m2 , but it has to be taken into account that a large proportion of the particles will produce no Cherenkov light because the particles are either below threshold or so close above it that the number of photons will be negligible (< 1) we get a number of particles above the effective Cherenkov threshold of 1180 corresponding to a density of 40 particles/m2. In the pattern recognition events that we ran in sect. 6-1 a higher density was successfully handled!

In table 1. we give the breakdown by charged particle species, primaries and secondaries produced in the RICH volume, reaching the MWPC.

TABLE I

Number of charged particles reaching the central ALICE RICH wheel for one event (dN/dY=8000 B=.2T)

particle species	# particles in RICH	particle species	# particles in RICH
e+	111	e-	113
μ+	167	μ-	129

$\pi+$	540	$\pi-$	516
K+	18	K-	23
p	118	p-	21

In conclusion, a satisfactory pattern recognition was achieved with a maximum density of tracks, all generating Cherenkov photons (pi/proton 3 GeV/c) and including a realistic background. That corresponds to a maximum density of hits, however keeping in mind that those tracks were all orthogonal to the detectors. On another hand, the GEANT simulation indicates that a sizeable fraction of tracks will generate less photons, reducing the hit density, but GEANT shows also that these tracks will deposit a larger ionization in the detector due to their large angle of incidence. The analog pad pulse height information will help to identify such events.

6- Study of a large liquid radiator array for the ALICE RICH barrel.

The RICH array in ALICE is being designed following the basic criterion to optimize the detector performance in terms of Cherenkov angle resolution. A modular construction is envisaged with sixty modules arranged around five "wheels" of approximately 3.6 m radius; each annular surface is tilted in such a way that the average direction of the incoming particles is almost perpendicular in every wheel. Fig. 23 shows a sectional and a 3-D view of the barrel as implemented in the general ALICE detector framework. Preliminary studies have been carried out on its implementation [18].

The good performance of the RICH depends strongly on the quality of its radiator, namely liquid C6F14, on the aspects of transparency and long term stability. Therefore emphasis has been put to the definition of the mechanical design for the radiator vessel.

Dimensions, weight, density and chemical resistance to C6F14 are the main constraints in designing the structure. The radiator vessel under study can be represented with a base panel of 170x170 cm2, presenting four ribs intersecting half way along the inner plane and four more ribs along the outer edges (Fig. 24). In this way nine independent volumes, of 50x50 cm2 and 10 mm depth, are obtained in which liquid C6F14 is circulated. These volumes are closed by nine windows of pure fused silica glasses of 51x51 cm2 , tightened to the rest of the structure by an additional frame. Optimizing the glass thickness is also part of this section.

Due to the rather high C6F14 and silica glass densities and the various orientations around the LHC beams, the radiator has been analyzed in terms of structure, load conditions and constraints.

The load, mainly the liquid and the quartz, acts on different elements according to the location of a module around the barrel-shaped RICH: in horizontal modules located at the top or the bottom of the barrel, the windows or the panels are uniformally loaded while a vertical module stands the hydrostatic pressure of the C6F14.

The vessel thickness has to be calculated as a trade off between minimizing the wall radiation length and the deflection due to Freon weight.The maximum vessel flexural deflection has been choosen to be 0.5 mm for two main reasons:

a) a maximum flexural deflection of 0.5 mm is an acceptable variation of the radiator thickness considering its contribution to the geometrical error in the evaluation of the Cherenkov angle;

b) a flexural deflection below 0.5 mm is necessary to avoid that structure deformations produce stress higher than the total bending stress in the quartz. In fact fused silica is brittle and may crack under flexural loads.

A composite honeycomb sandwich has been chosen to construct the panel. The inner core is made of three layers reinforced by two intermediate thin glass fiber foils. The selected materials are diamagnetic and stable in presence of C6F14 to avoid any pollution that could cause drop in the transparency of the liquid in the 160-220 nm band. To optimize stiffness versus density, a seven layers sandwich has been considered using the following components:

- Carbon fiber outer skins: two foils of CIBA-GEIGY Vicotex 1454,
- Honeycomb core: three layers of AEROWEB type A1 (polyamide)
- Glass fiber inner layer: two foils of Vicotex 1131.

Their thicknesses,listed in a table below are t, c, h respectively

The study of constrains and deformations developed in the system required an approach based on finite element analysis. The evaluation was done on a module in a vertical position providing the most peculiar and demanding load conditions. The ANSYS 5.A package running on a HP 9000/730 workstation with a risc architecture bas been used for this evaluation.

In order to optimize the thickness of the quartz window, the SHELL 63 structural element with a grid mesh of 12.5 mm has been adopted. Each window is supposed to be framed with four fixed edges. The results are summarized :

s [mm]	f [mm]	σ [MN/m2]
4	0.868	23.6
5	0.444	15.1
6	0.257	10.5

with s, f, σ being the thickness, the maximum deflection and the maximum stress, respectively.

It can be noticed that using a 6 mm thickness a good compromise between deflexion and maximum stress is obtained since the quartz bending strength is 67 MN/m2. Further studies to reduce that thickness by means of inserts between the base plate and the window are in progress.

To model the sandwich panel structure, the structural layer SHELL 99 has been adopted using a grid mesh of 50 mm. A typical set of results is summarized:

c [mm]	h [mm]	t [mm]	f [mm]	σ [MN/m2]
20	0.5	0.5	1.443	20.7
30	0.5	0.5	0.564	11.6
40	0.5	0.5	0.396	9.25
50	0.5	0.5	0.264	7.0

The finite element analysis shows that there are little differences in terms of maximum deflection using different core material, directing the choice on the material of lower density. Moreover, to prevent possible pollution effects due to the C6F14, a protective foil of 0.1 mm thick aluminium will be bonded on the carbon fiber layer, of negligeable contribution to the total density.

The C6F14 inlet and outlet piping is implemented without any couplings; the feed tubes are embedded in the container walls to reduce leakage risk.

Furthermore, the design and the realization of a reduced scale prototype will be considered in order to gain useful information on its mechanical stability and the behaviour of the vessel wall to the incoming particles in terms of secondary interactions. The radiator will be filled with C6F14 to study the UV transparency over long periods of time.

The second component of a RICH module is the photon detector consisting of a MWPC. The structural problems are much less severe. The wire chamber will be composed of several frames and the pad cathode made also of a composite honey comb panel. The problems related to the frontend pad electronics implementation and connection have been solved on our different prototypes achieving an overall density equivalent to 3% of a radiation length. The CsI evaporation on such panels is also well mastered. The next engineering effort will be put on the design of a cost effective layout of the chamber.

7- Development of the VLSI pad electronics.

7-1 VLSI analog frontend chip, 16 channels: GASSIPLEX

That chip has been developed with the same internal circuitry as the GASPLEX [19], using a 1.5 μm C-Mos technology. It is composed of i) a charge sensitive preamplifier, ii) a dedicated filter which cancels the slow part of the input signal given by the ion motion in a gas detector, iii) a pulse shaper which insures a good return to the base line allowing for high counting rates, illustrated by typical pulse shapes shown in fig. 25. The new chip has the same external functionalities as AMPLEX [14].

At 5 mW/channel of power consumption, the following features were measured: i) input noise: 650 electron rms ECN at 0 pF, ii) noise slope: 14 electron/pF, iii) sensitivity: 12.2 mV/fC, iv) linear dynamic range: 0 to +2V (180 fC), 0 to -1.2V (100 fC), v) adjustable peaking time from 400 to 700 ns, vi) base line return: better than 0.5% after 4 μs, vii) readout clock rate: up to 10 MHz.

7-2 VLSI general chip, 16 channels: DIGITPLEX

As shown in fig. 26, the goal of the DIGITPLEX circuit is to provide the main elements of the traditional analog readout channel for particle detectors on a single chip, using a 0.7 μm technology [20]:

- a charge preamplifier followed by a pulse shaper matched either to wire chamber or to silicon detector input current shapes,
- a track/hold and an analog multiplexer,
- an analog to digital converter followed by a digital circuitry which performs the data cleaning: zero skipping, pedestal substraction, and local memorisation of the good data to ease their transfer to a central data acquisition and allow a sparse readout mode

The expected performance is:

i) input noise: 450 electron rms ECN at 0 pF with a slope of 12 electron/pF
ii) internal analog clocking at 10 MHz,
iii) 4-ranges ADC on 8 bits with 1 mV accuracy on the first range and 2.048V maximum on the highest range, 10 MHz clocking,
iv) zero skipping by comparison to threshold map, pedestal substraction, four events FIFO memory, 20 MHz data readout clock.

7-3 Status of the development.

The GASSIPLEX chip, version 1.5 μm, is under production and a thousand of channels will be in operation, in particular at the NA44 experiment.

That chip, serving as the analog block of DIGITPLEX, is being converted into a 0.7 μm technology chip to be evaluated. Then, full DIGITPLEX prototypes are expected for mid-1995 in case of acceptance of the analog frontend.

8- Summary, conclusion and proposal for 1995

In 1994, the main steps towards the achievement of our milestones can be summarized as follows:

1- operation of a fast RICH with large CsI photocathodes

i) demonstration of a specific processing of the CsI layer to achieve a high standard value of the QE in the 160-210 nm range, the basic features being;

• heating at 60°C during and after the evaporation (4-5 hours)

• polished substrate with a metallic layer (Ni or Ni/Au) avoiding contact between CsI and copper in case of large area photocathodes segmented into pads.

A good reproducibility was observed on small samples. A proof of principle was given by five large area PCs achieving 70-90% of the standard QE performance.

ii) stable operation of a fast CsI-RICH detector achieving:

• 14 photoelectrons/ring from a 10 mm thick C6F14 radiator with 3 GeV/c pions, expected to reach 16-18/ring with optimized grid transparencies and final electronics

• angular resolution for single photoelectron of 8 mrad at 100 mm ring radius

• negligible contribution of the photon feedback in a fully open MWPC geometry in pure methane at a gas gain up to 1.0 10E5

• 2-dimensional localization of single electron with a detection efficiency of 80-90% using analog multiplexed frontend electronics

• localization of the incoming charged particles with an rms accuracy < 0.5 mm

iii) stability of the QE performance after an exposure of the CsI layer to air up to 45 minutes

iv) possible use of gas mixtures with low hydrocarbon content preserving the QE performance (argon/i-C4H10)

2- pattern recognition and particle separation with density of 50 particles/m2 (ALICE)

i) pi/K 3 sigma separation up to 2.6 GeV/c from pad patterns obtained by overlapping test beam events, background included, up to a density of 50 particles/m2

ii) realistic RICH layout implemented in the ALICE GEANT simulation

3- ALICE barrel RICH: layout and electronics

i) preliminary study of a barrel RICH structure and definition of the detector modules

ii) preliminary study of a large array of liquid C6F14 radiator

iii) design and production of a new VLSI chip, GASSIPLEX as an analog multiplexed frontend for pad readout

iv) development of the final pad readout chip, DIGITPLEX, including 8 bits digitization on chip and allowing for sparse data readout mode.

During that second year, the main developments and results achieved by the RD26 collaboration have been issued in publications found under references 4, 6, 7, 8, 9, 10, 11, 12, 13, 18 and presented at the Elba, Como and IEEE, Norfolk conferences.

The results obtained this year converge for the first time towards a demonstration

that a fast RICH can be safely operated with a large CsI photocathode of aQE largely satisfying the particle separation required at ALICE. The pattern recognition has also been found achievable at densities up to 50 particles/m2 with a background contribution measured with single particles.

We want to stress that the design of such a second generation RICH detector has become largely simplified, as it is composed of a radiator array and a classical MWPC. The detector is intrisically 2-dimensional and has a thin sensitive volume resulting in a reduced background even in a high density of particles.

In the description of the performance in identification of particles of the present prototype, we refer to the performance asked by the LHC-ALICE collaboration from such a detector. However, it is obvious that at low particle densities and using larger gaps pi/K separation at much higher momenta may be achieved. The limited rate capability of the electronics in low density events should not be a too serious limitation for interaction rates up to 10E5 Hz. In fact, such environment will be met at HADES/SIS in a near future.

The significant breakthrough in QE of large CsI PC incorporated in MWPC's as well as the better understanding of related phenomena require a final demonstration of the construction and operation of a prototype of larger size than the ones used so far, allowing for multiparticle detection in conditions similar to those expected in ALICE. We therefore request an extension of one year with the following programme:

1- Using the existing RD-26 facilities and prototypes:
- test the reproducibility of high QE large photocathodes (test beam : PS/T11)
- test the ageing properties with and without exposure to air
- in-depth laboratory studies of the heat treatment consequences
-furtherv studies of gases in terms of photoemission and feeback

2- Final ALICE-like module prototyping:
- construction of a 1 m2 prototype equipped fully on a surface of 0.5 m2 with radiators and electronics (Gassiplex and finally some Digitplex)
- test of the prototype in a multiparticle environment, using the test beam facility to be installed for ALICE at the PS (see below)

The proposed programme requires the following contributions from CERN:

1- Partial financial support for the building of the 1m2 prototype according to the 1995 CERN budget request amounting to 150 kSF. The CERN group should take charge of the building of the photo detector and part of the electronics,

2- Use of the test beams: presently discussions are underway to organize a test facility at the PS/East area for the ALICE users. We intend to use this facility with proton beams on heavy targets to have multiparticle hits in the RICH. Also, the possible implementation of a primary Pb line in that zone is under evaluation for 1996. In 1995, our overall beam time at the East area is evaluated at 8-10 weeks.

The other collaborating institutions have also agreed to continue the financing at a level equal to the one in the past two years.

Acknowledgments

The RD26-CERN group wants to warmly acknowledge his CERN colleagues for their essential contributions: Mr. D. Carminati, taking charge of the numerous CsI evaporations, Mr. A. Gandi and his staff for the elaboration of the new pad substrates, Mr. J.P. Bacher and J.M. Dalin for the SEM and X-ray studies, Mr K. Batzner and L. Durieu for their help in running the PS/T11 test beam.

References.

[1]- J. Seguinot et al. Nucl. Instr. and Met. A297 (1990) 133
[2]- D. Anderson et al. Nucl. Instr. and Met. A323 (1992) 626
[3]- A. Braem et al. Fast RICH detector with a CsI photocathode at atmospheric pressure. Nucl. Instr. and Met. A343 (1994) 163
[4]- J. Almeida et al. Development of large area fast RICH prototypes with pad readout and solid photocathodes. Nucl. Instr. and Met. A297 (1994)216
[5]- A. Breskin et al. A corection to the QE of CsI and other photocatodes due to the recalibration of the reference photomultipliers. Nucl. Instr. and Meth. A343 (1994) 159
[6]- A. Breskin et al. Electric field effects on the QE of CsI photocathodes in gas media Nucl. Instr. and Meth. A344 (1994) 537
[7]- A. Breskin et al. Field-dependent photoelectron extraction from CsI in different gases. Submitted to the 1995 Wire Chamber Conference, Vienna. In preparation.
[8]- A. Buzulutskov et al. Field-enhancement of the photoelectric and secondary electron emission from CsI. Preprint WIS-94/11/Feb.. J. of Applied Phys. In press.
[9]- A. Buzulutskov et al. New ideas in CsI-based photon detectors..Preprint WIS-94/47Oct. Presented at the 1994 IEEE NSS, Norfolk. To be published in IEEE Trans. NS.
[10]- A. Almeida et al. Microanalysis surface studies and photoemission properties of CsI PCs. Submitted to the 1995 Wire Chamber Conference, Vienna. In preparation.
[11]- Ph. Miné et al. Incident angle effect on the QE of CsI PCs. Presented at the 6th Pisa meeting on Advanced detectors, Elba, May 1994 , Nucl. Instr. and Meth. in press.
[12]- A. Akkerman et al. Low- energy electron transport in alkali halides. J. of Appl. Phys. 76 (1994) 4656
[13]- J. Almeida et al. Morphological effects on CsI quantum yield, to be published in Surface Science
[14]- E. Beuville et al. Nucl. Instr. and Meth. A288 (1990) 157
[15]- J. Séguinot, private communication
[16]- A.Ljubicic Jr et al. Current Status of the RICH Monte-Carlo and Analysis", ALICE Collaboration meeting, Jan. 1994.
[17]- A.DiMauro et al. Particle identification with a solid cathode RICH in ALICE at LHC. Nucl. Instr. and. Meth. A, 343 (1994) 284
[18]- A. Di Mauro et al. Design of a large area fast RICH with CsI photocathode for particle identification at ALICE-LHC. Presented at the Conference on Advanced Technology and Particle Physics, Como, Oct. 1994 , Nucl. Instr. and Meth. in press.
[19]- P. Jarron et al. CERN/ECP/MIC 94-17
[20]- J.C. Santiard et al. CERN/ECP/MIC 94-note1

Figure captions

Fig. 1- Temperature enhancement of the QE of CsI as function of time, measured under vacuum with a UV monochromatic light beam.

Fig. 2- QE of CsI versus wavelength. The two upper graphs are "best results" while the two lower ones represent results averaged over many samples and measurements.The "Weizmann" result is taken as the "RD26 reference" QE .

Fig. 3- Relative variation of the QE of CsI measured under gas as function of E/p: in a), with He/i-C4H10 and He/CH4, a first plateau (collection mode) is observed at low E/p values to reach a second one (multiplication mode) at higher E/p, corresponding to the QE value in vacuum; in b), with CH4/i-C4H10 the full QE value (the vacuum value) is already reached at low E/p values (collection mode)

Fig. 4- Normalized QE of CsI as a function of the electrical field strength in vacuum, measured on a thin wire photocathode. Note the 25-fold enhancement reached above 200 nm at 500kV/cm.

Fig. 5- Variation of the QE of each cone normalized to that of a flat photocathode from the same batch.

Fig. 6- Comparison between a simulated QE graph of CsI and the RD26 reference.

Fig. 7- Scanning Electron Microscope (SEM) images of CsI layers deposited on a) G10/Cu/Au chemical, b) G10/Cu polished/Ni/Au, c) G10/Cu polished/Sn. A dis ordered and inhomogeneous grain growth is observed in a) becoming regular in b),c).

Fig. 8- Photoemission Electron Microscope (PEEM) images (from a Deuterium lamp) of CsI layers deposited on c) G10/Cu/Au chemical, b) G10/Cu polished/Ni/Au, a) G10/Cu polished/Sn, d) Aluminium. High emission yields (bright images: a,b) are obtained on the new substrates compared to the low yield (dark image: c) on the old one. The same homogeneous morphologies as the SEM ones are observed in the PEEM images.

Fig. 9- Photoemission Electron Microscope (PEEM) images (from ESCA) of CsI layers deposited on Al comparing primary emission of Cs (b) to I (c) and showing a Cs/I segregation: the bright regions correspond to areas of stronger emission

Fig. 10- Sectional schematic view of the CsI- fast RICH prototype

Fig. 11- Influence of the pad size (8x8mm2) on the photoelectron overlap fraction for different ring radii as a function of the number of photoelectrons per ring.

Fig. 12- Single Cherenkov ring events of 100 mm radius: the axies are in units of pad length (8mm).

Fig. 13- Main results of the CsI- fast RICH's using the G10/Cu/Ni pad electrodes: a) small RICH, 38 mm ring radius; b) large RICH, 98 mm ring radius. The measurements are compared to the simulation.

Fig. 14- QE of CsI graphs used to fit data to the simulation compared to the RD26 reference (full line). The two upper curves delimit the QE obtained with the five CsI PCs using the new substrate. The hatched area correspond to PCs using the old ones.

Fig. 15- Angle distributions of single Cherenkov photoelectrons and background events measured in the CsI fast RICH using as gas mixtures: a) methane, b) argon/methane 80/20. Note the increased photon feedback background contribution in b).

Fig. 16- Mean total pad PH/ring versus single electron mean PH (or amplification) for two radiator thicknesses. Measurements are compared to simulation.

Fig. 17- Angle distributions of single photoelectrons in the Cherenkov fiducial zone. Angles are obtained in a) from cluster centroids, in b) from the centre of every pad hit.

Fig. 18- Variations of the mean ring radius versus radiator thickness for two proximity gap widths. The measurements are compared to simulation.

Fig. 19- Variation of the QE measured with UV light over long time period (two PCs)

Fig. 20- Pad PH distributions of single electrons compared to exponential fit measured in a) methane and b) argon/methane 80/20.

Fig. 21- Four typical events from the superposition procedure. The density of particles is ~44 particles/m2 which would correspond roughly equivalent in occupancy to a 50 particles/m2 ALICE event, due to the fact that we are using only 3.0 GeV/c particles in the superposition. Note that no time was spent in choosing these 4 examples. They come from the first 40 consecutive events from the data acquisition at the test beam.

Fig. 22 : a) results of the analysis of single-ring events with 3.0 GeV/c momentum. The pion:proton ratio was artificially raised to 70:30. The proton angle corresponds to an angle which a 1.5 GeV/c kaon would have in the present detector setup.
b) results of the analysis of high-density events with 3.0 GeV/c momentum.The RMS of 7.0 mrad would correspond to a 3-σ K/pion separation at 2.6 GeV/c.

Fig. 23- Barrel RICH at ALICE: a) sectional view of a quarter of the barrel showing the orientations of the RICH modules in the wheels; b) artist view of the barrel structure.

Fig. 24- Liquid C6F14 radiator array of an ALICE RICH module: a) radiator segmentation (170 cm side); b) detailed section of the radiator

Fig. 25- Signal shapes measured with the chip GASSIPLEX connected to a pad MWPC showing: a) the good return to the base line level at two time scales, b) the effect of the filter on the return to the base line level (upper graph: no filter)

Fig. 26- Schematic functional diagram of the VLSI chip DIGITPLEX.

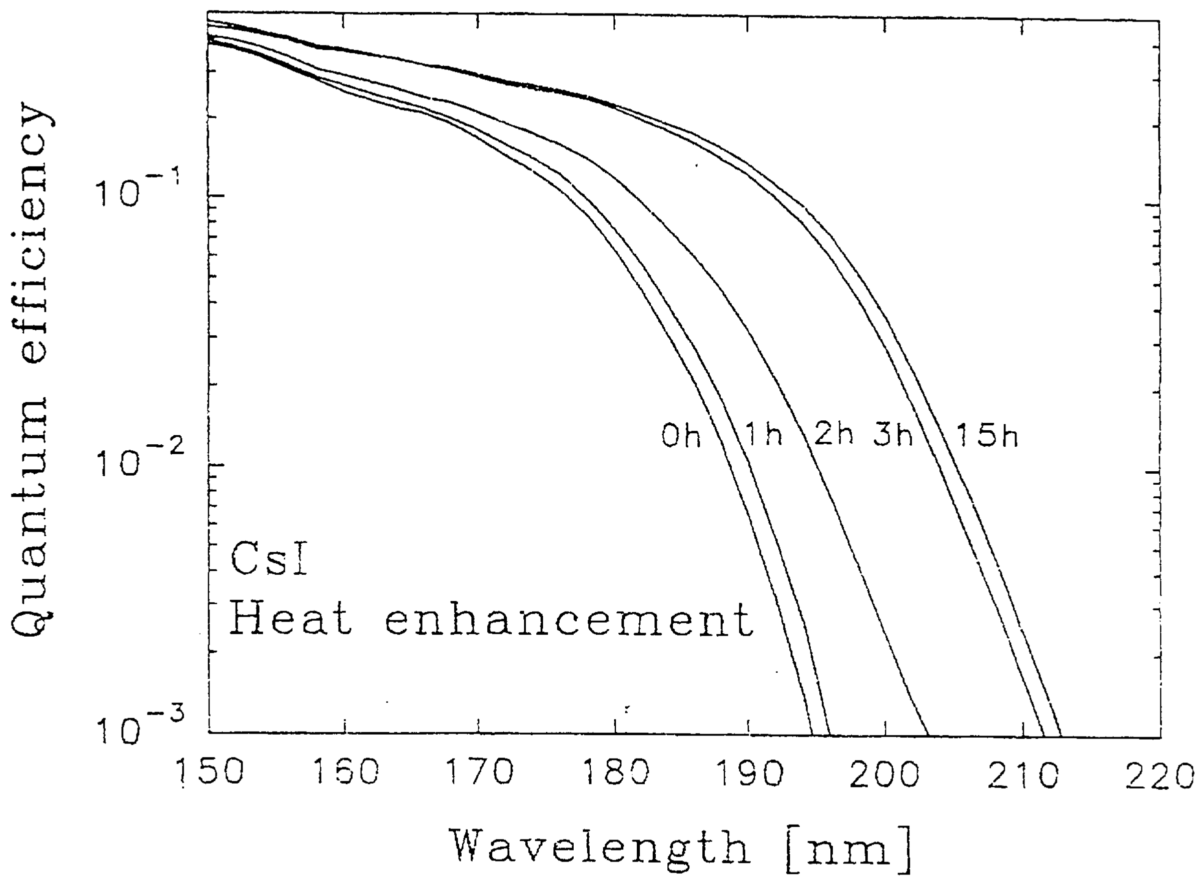

Quantum efficiency
10^{-1}
10^{-2}
10^{-3}
0h 1h 2h 3h 15h
CsI
Heat enhancement
150 160 170 180 190 200 210 220
Wavelength [nm]

Fig. 1

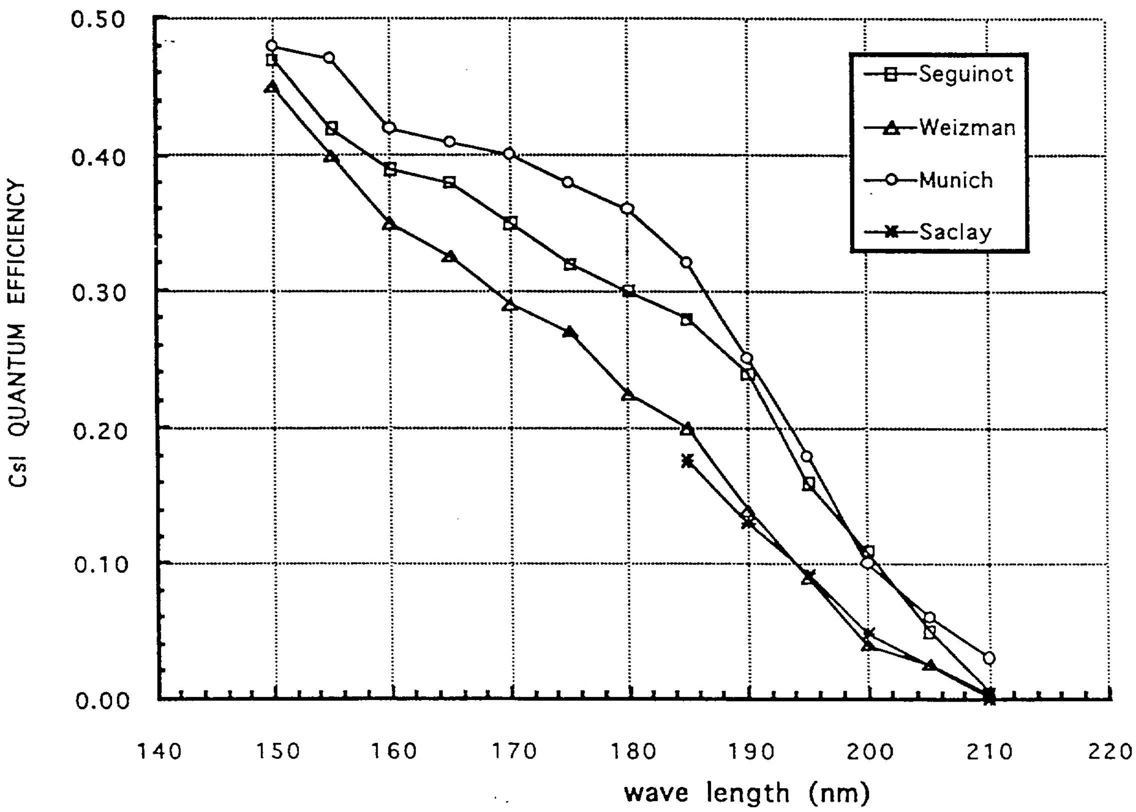

CsI QUANTUM EFFICIENCY
0.50
0.40
0.30
0.20
0.10
0.00
Seguinot
Weizman
Munich
Saclay
140 150 160 170 180 190 200 210 220
wave length (nm)

Fig. 2

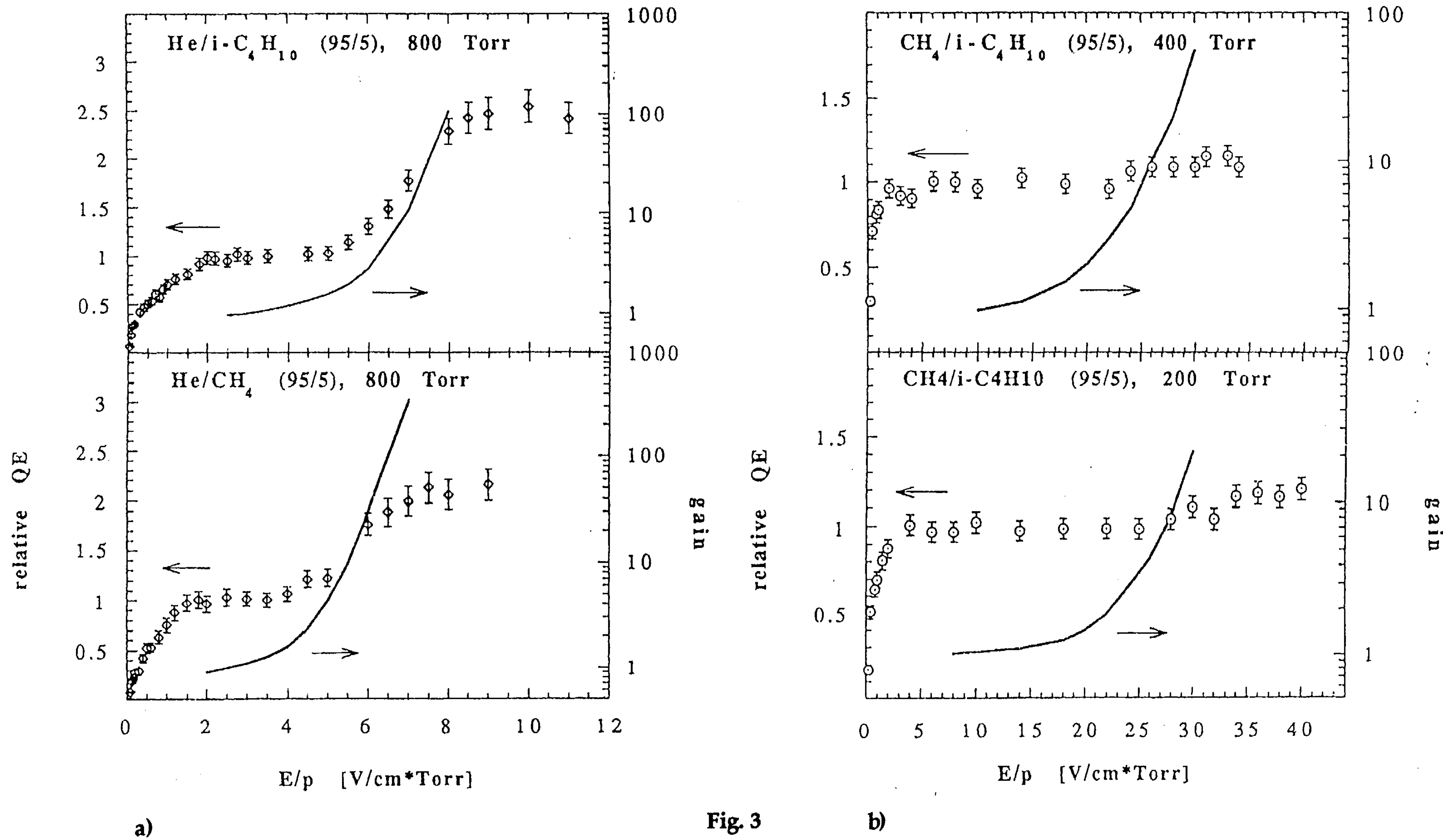
He/i-C4H10 (95/5), 800 Torr
He/CH4 (95/5), 800 Torr
CH4/i-C4H10 (95/5), 400 Torr
CH4/i-C4H10 (95/5), 200 Torr
relative QE
gain
E/p [V/cm*Torr]
a)
b)

Fig. 3

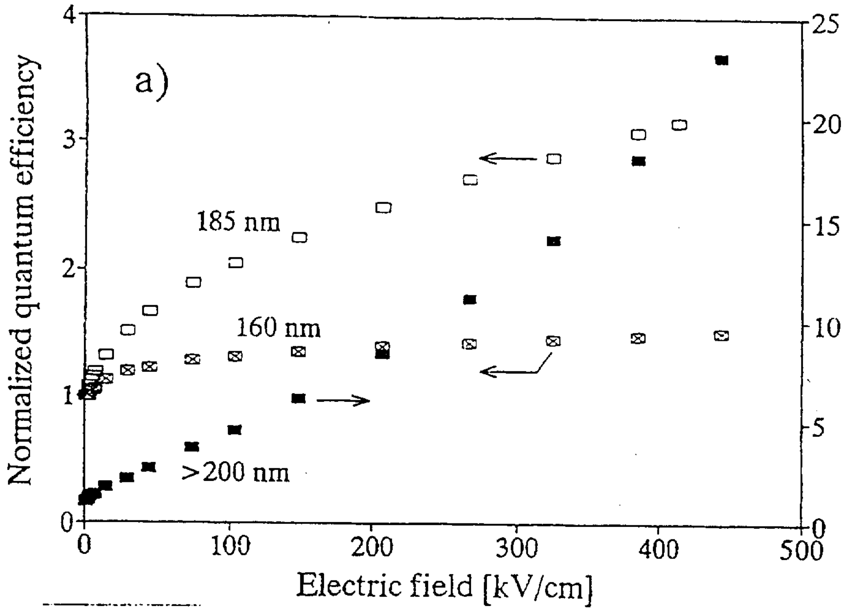

Fig. 4

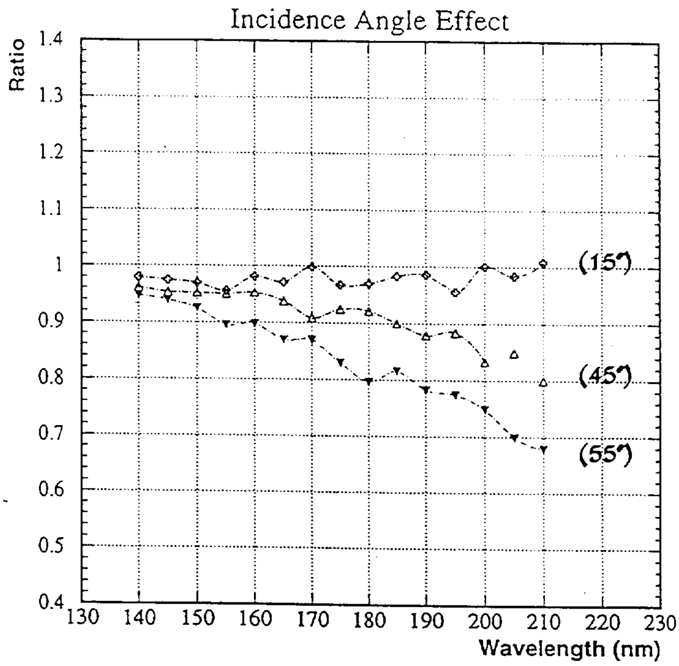

Fig. 5

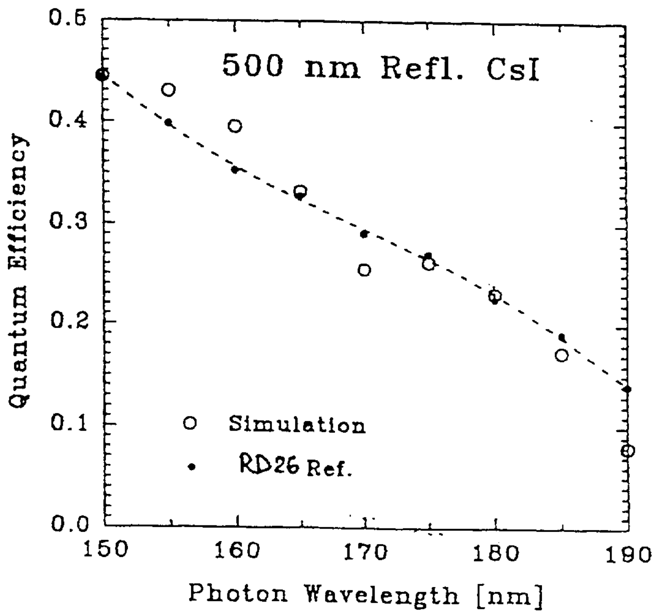

Fig. 6

Fig. 7

DEPOT DE CsI,SUR VETRONITE STANDARD,
JSHC, 500nm

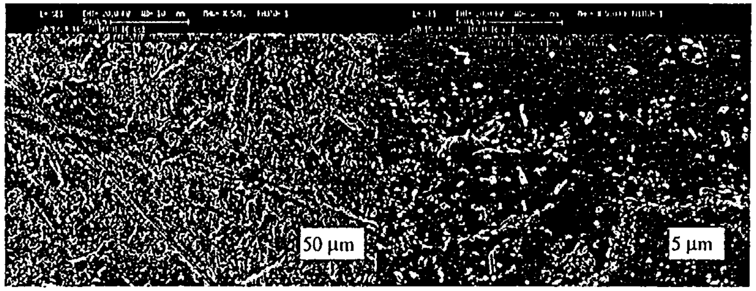

a)

DEPOT DE CsI SUR VETRONITE
+ CUIVRE + NICKEL + OR CHIMIQUE,
JSHC, 500nm

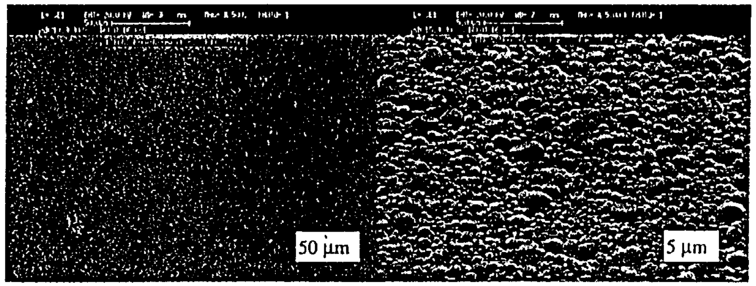

b)

DEPOT DE CsI,SUR VETRONITE ETAMEE,
JSHC, 489nm

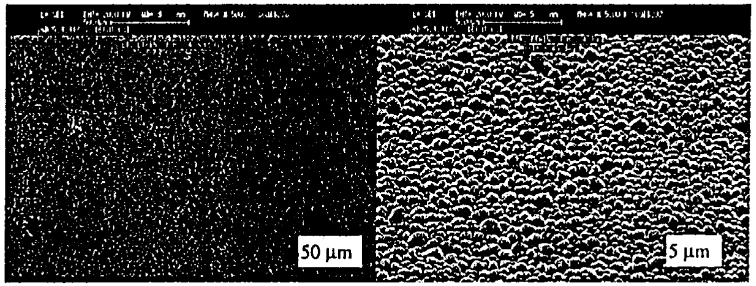

c)

Deuterium lamp

a) CsI (491nm) on G10 + Sn (JSHC)

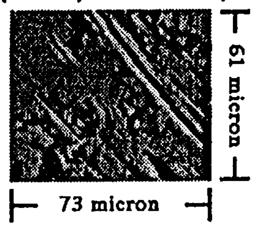

c) CsI (309 nm) on G10 + Au (EPC)

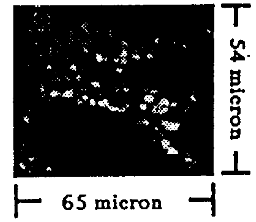

b) CsI (501 nm) on G10 + Ni-Au (JSHC)

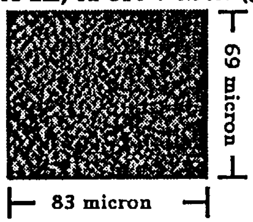

d) CsI (501 nm) on Al (JSHC)

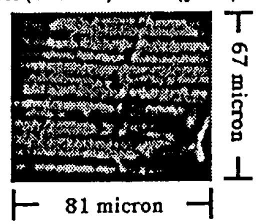

Fig. 8

CsI (501 nm) on Al

a)

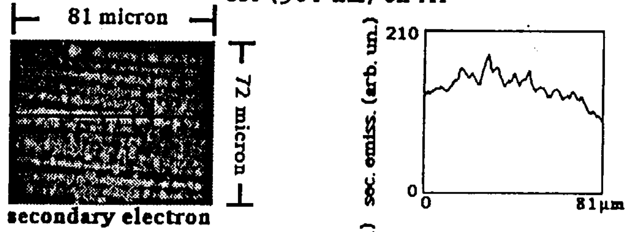

b)

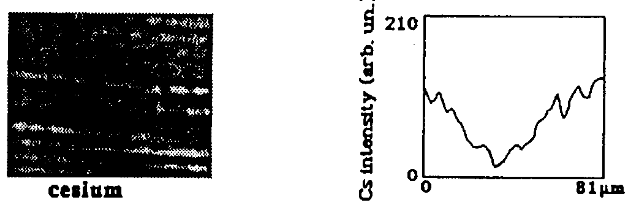

c)

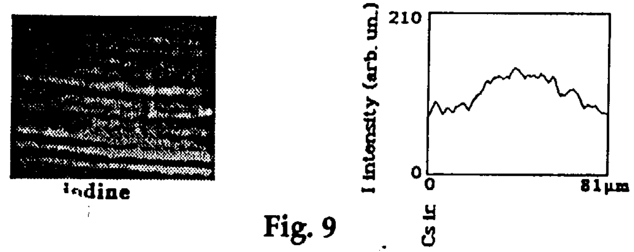

Fig. 9

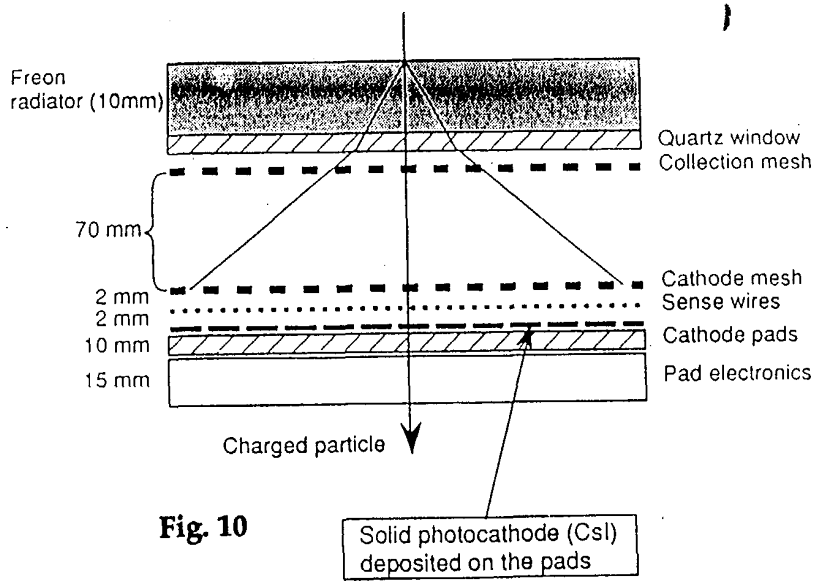

Fig. 10

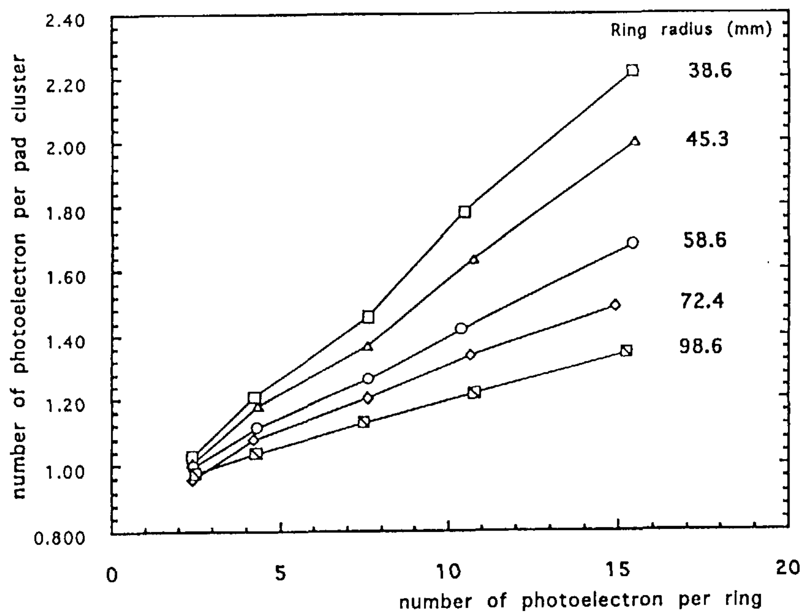

Fig. 11

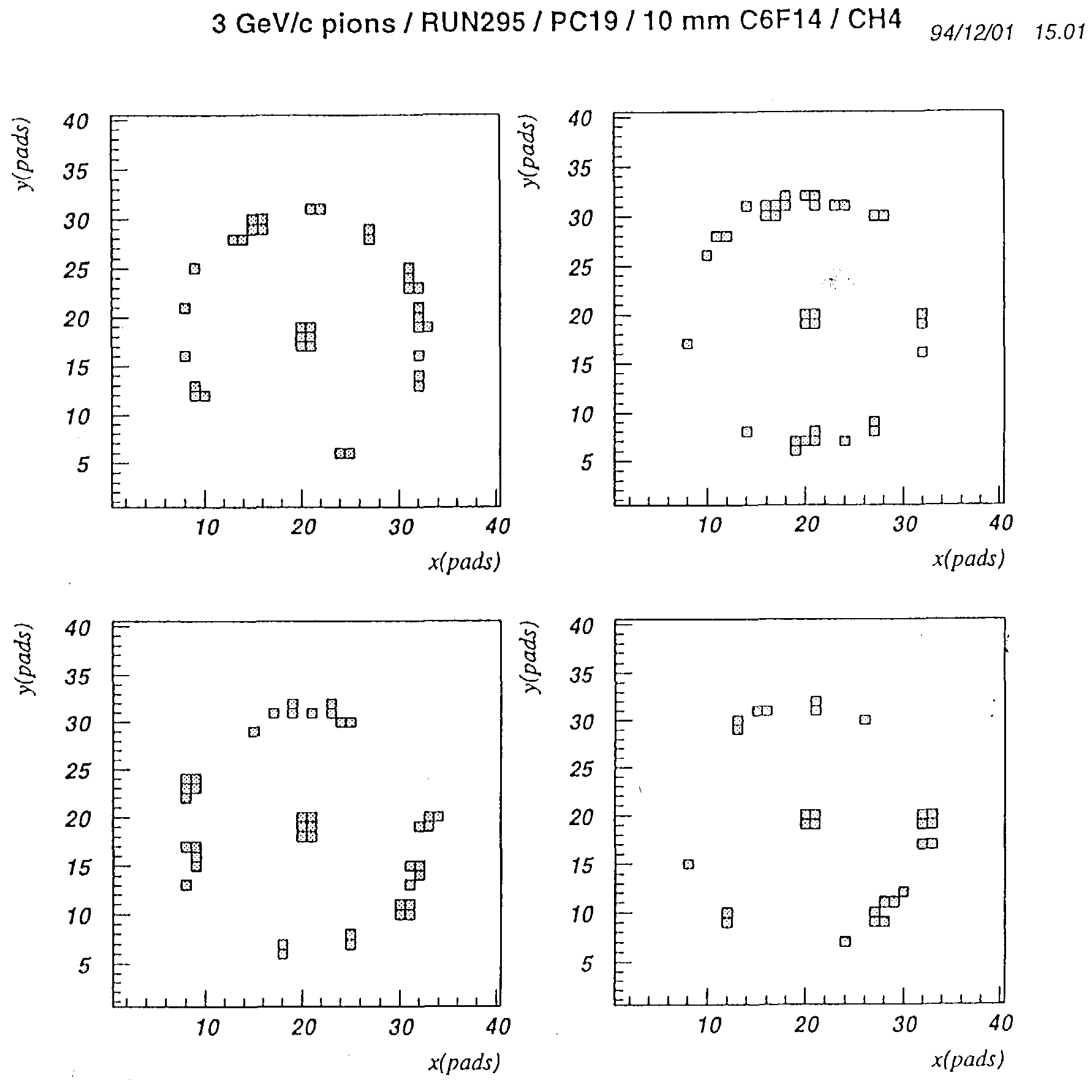

Fig. 12

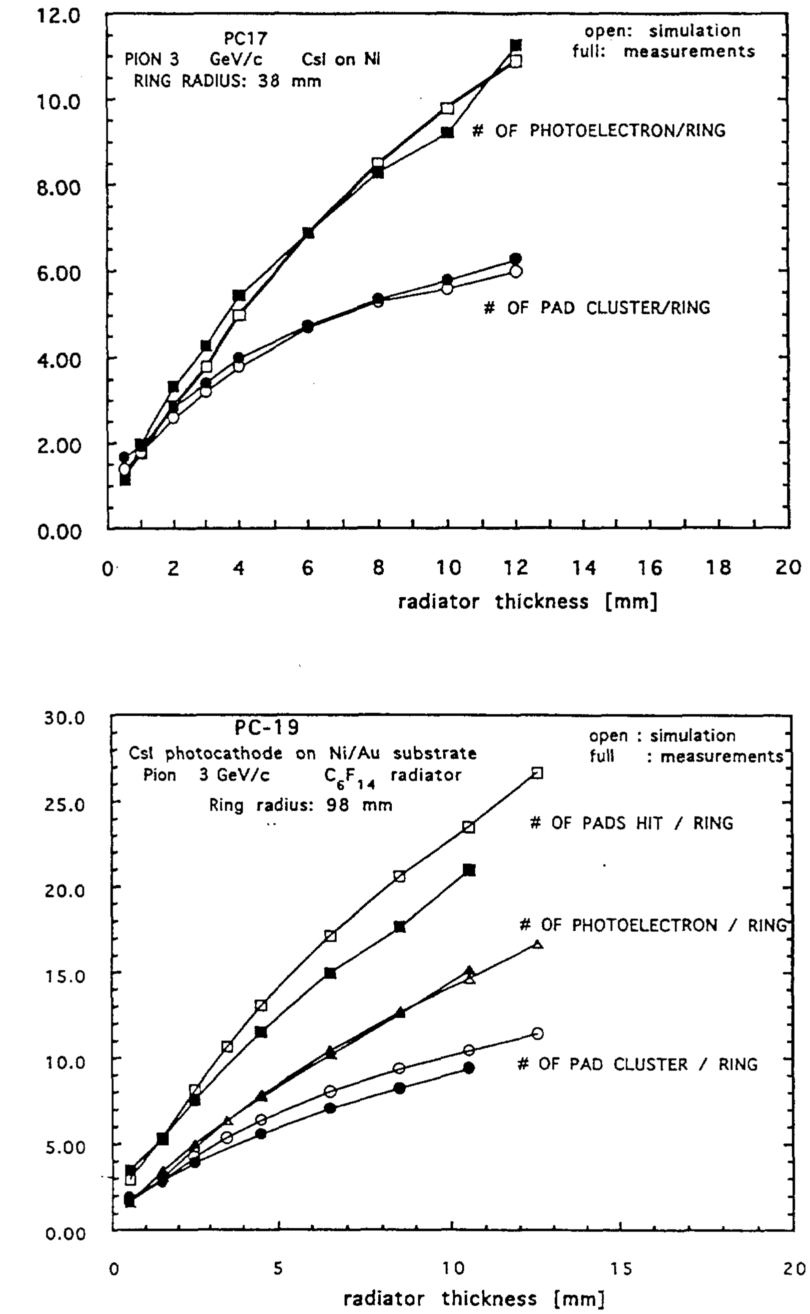

a)

b)

Fig. 13

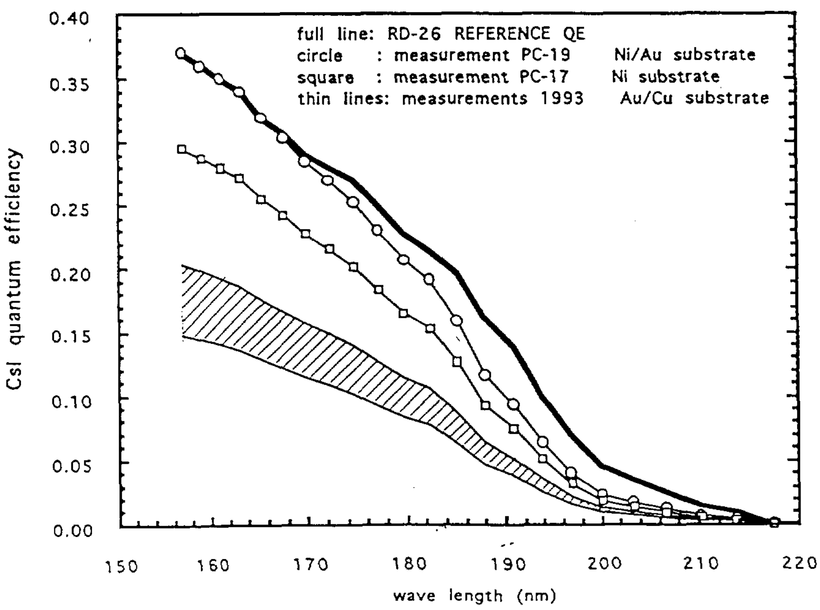

Fig. 14

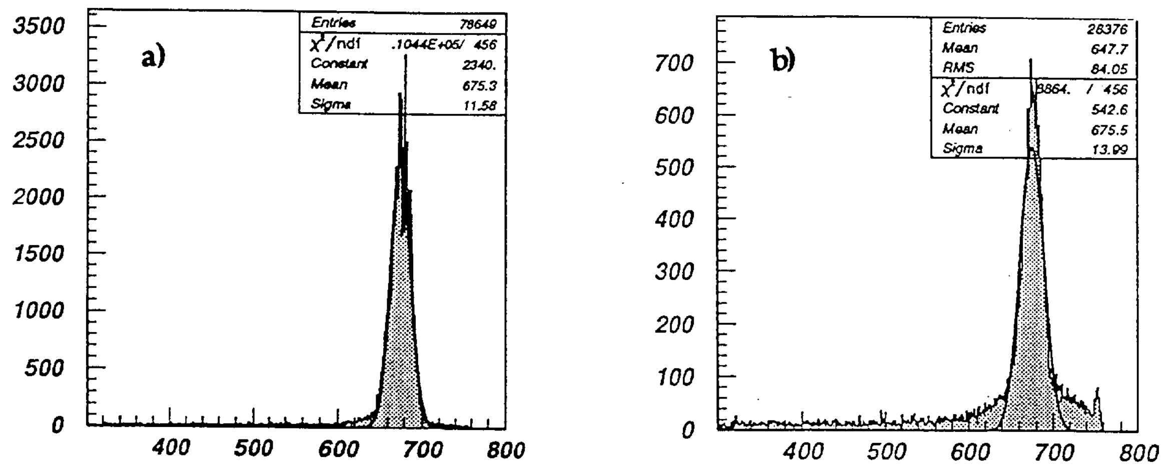

Fig. 15

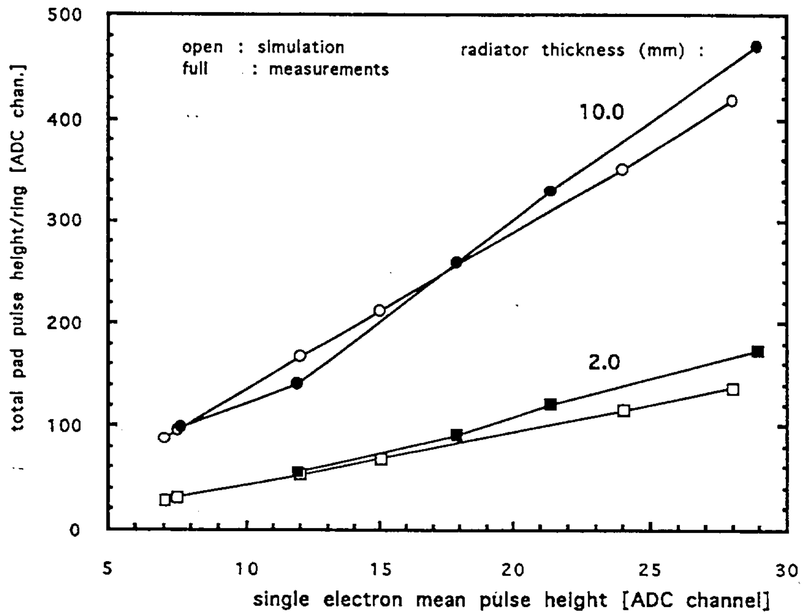

Fig. 16

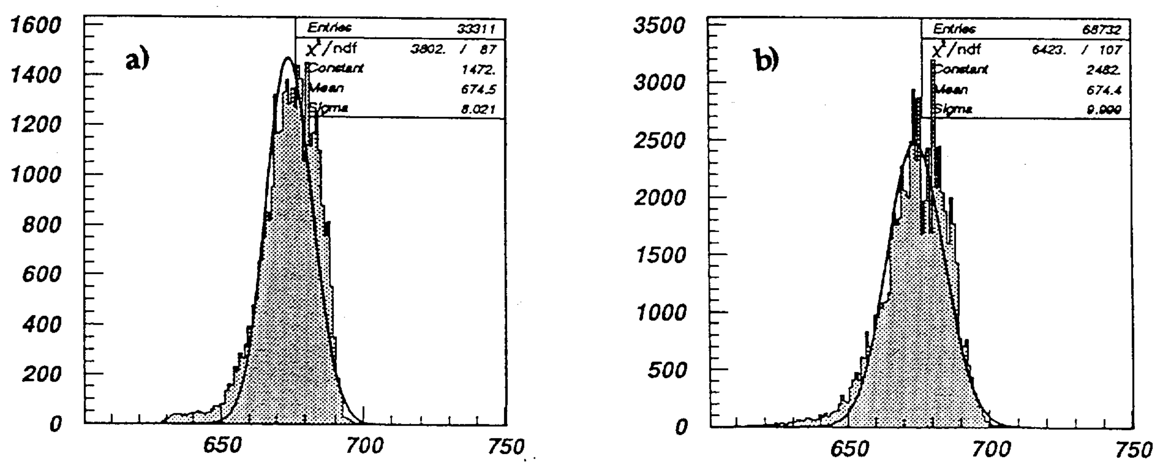

Fig. 17

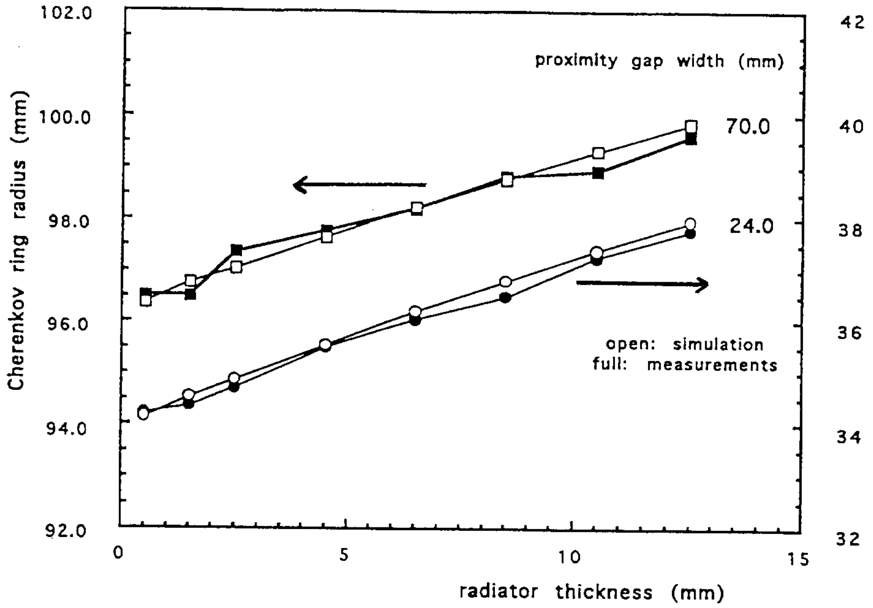

Fig. 18

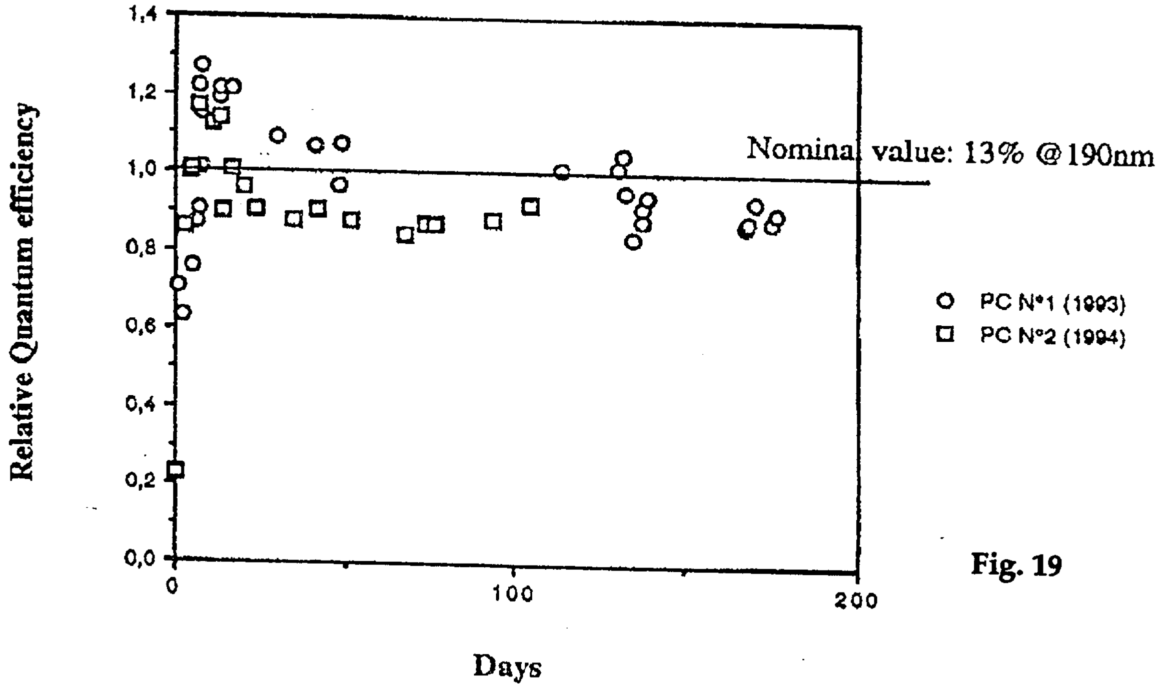

Fig. 19

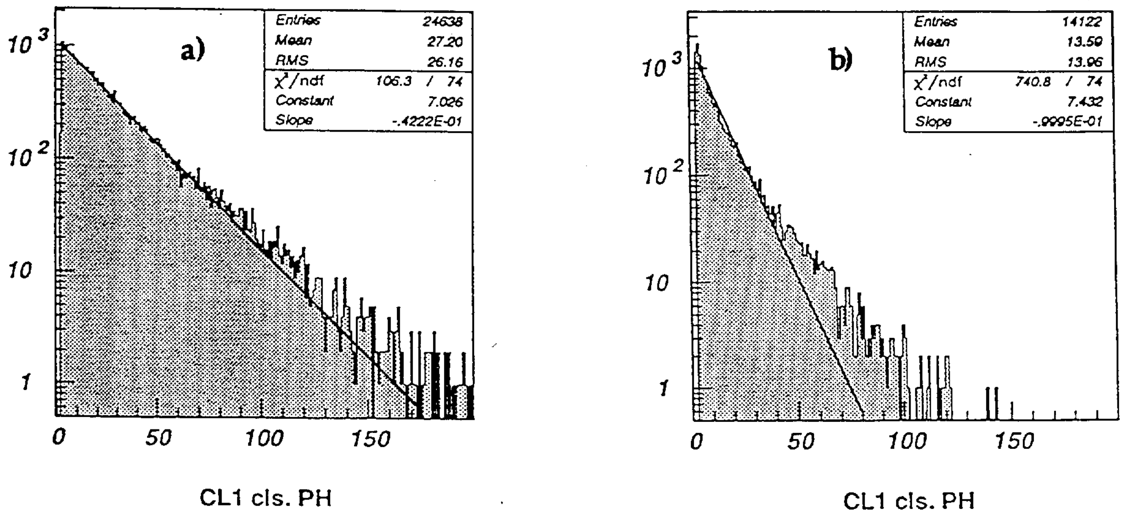

Fig. 20

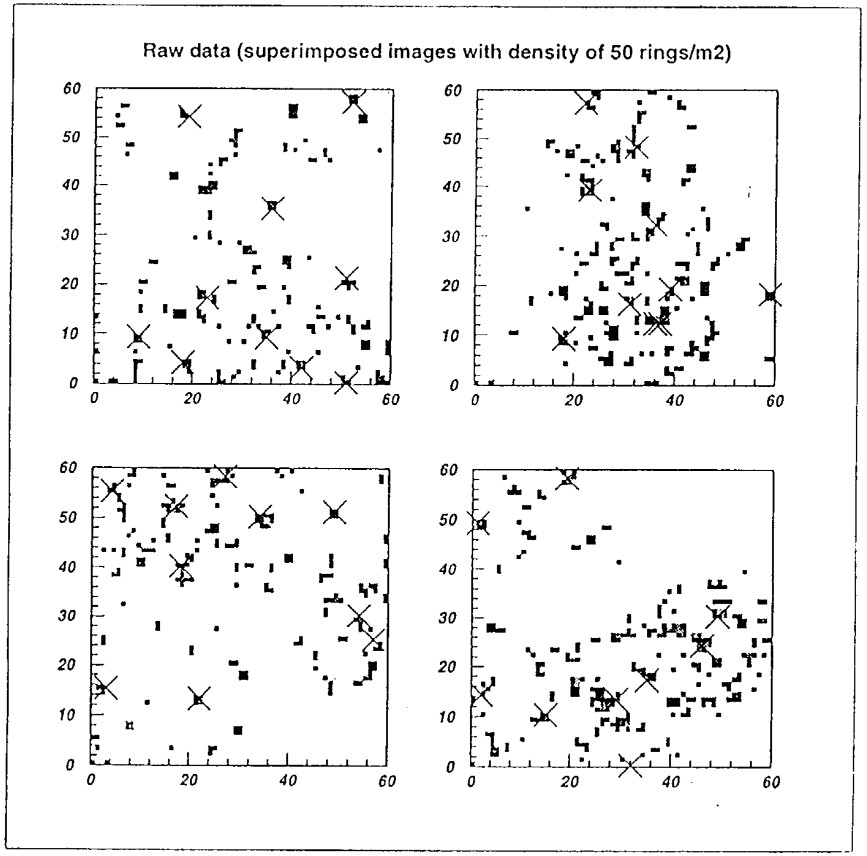
Raw data (superimposed images with density of 50 rings/m2)
0
20
40
60
0
10
20
30
40
50
60

Fig. 21

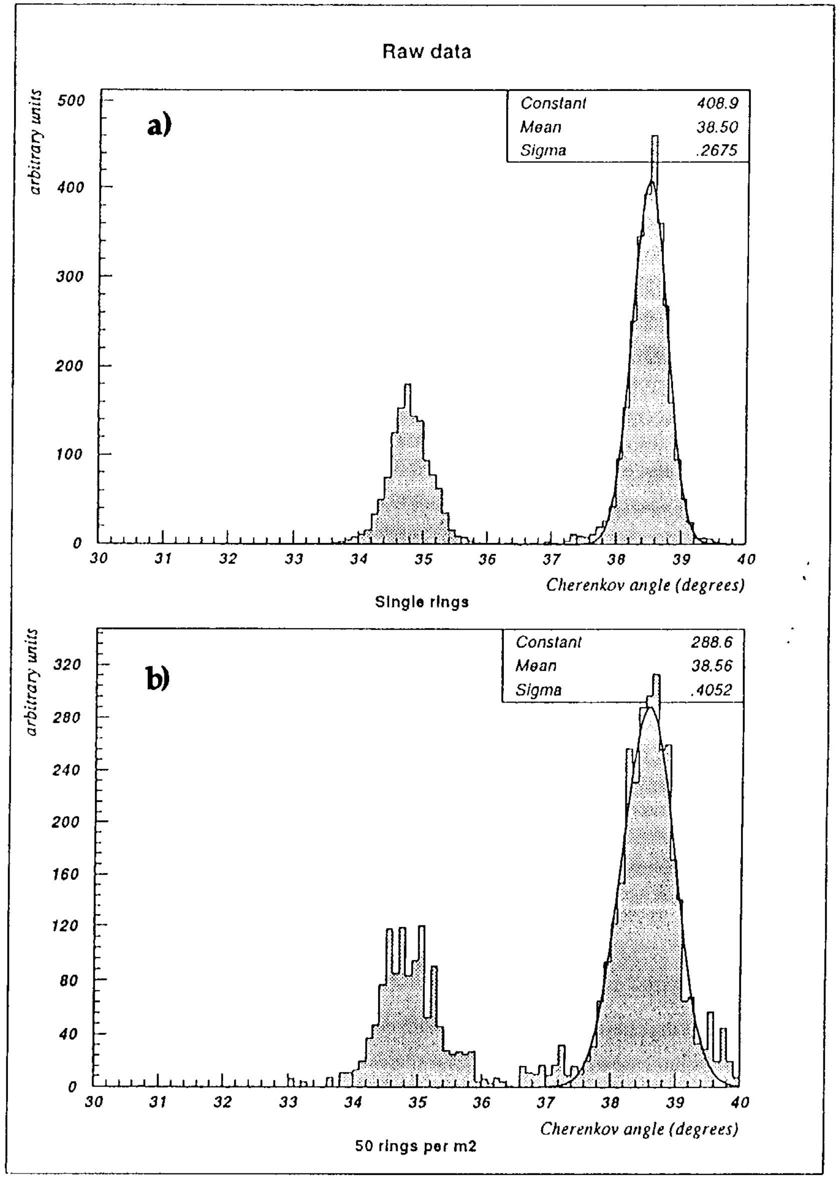
Raw data
a)
Constant 408.9
Mean 38.50
Sigma .2675
arbitrary units
Cherenkov angle (degrees)
Single rings
b)
Constant 288.6
Mean 38.56
Sigma .4052
arbitrary units
Cherenkov angle (degrees)
50 rings per m2

Fig. 22

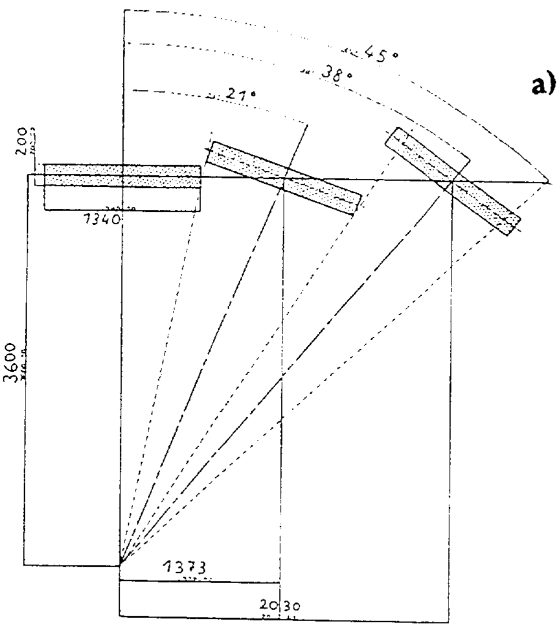
a)
45°
38°
21°
200
1340
3600
1373
2030

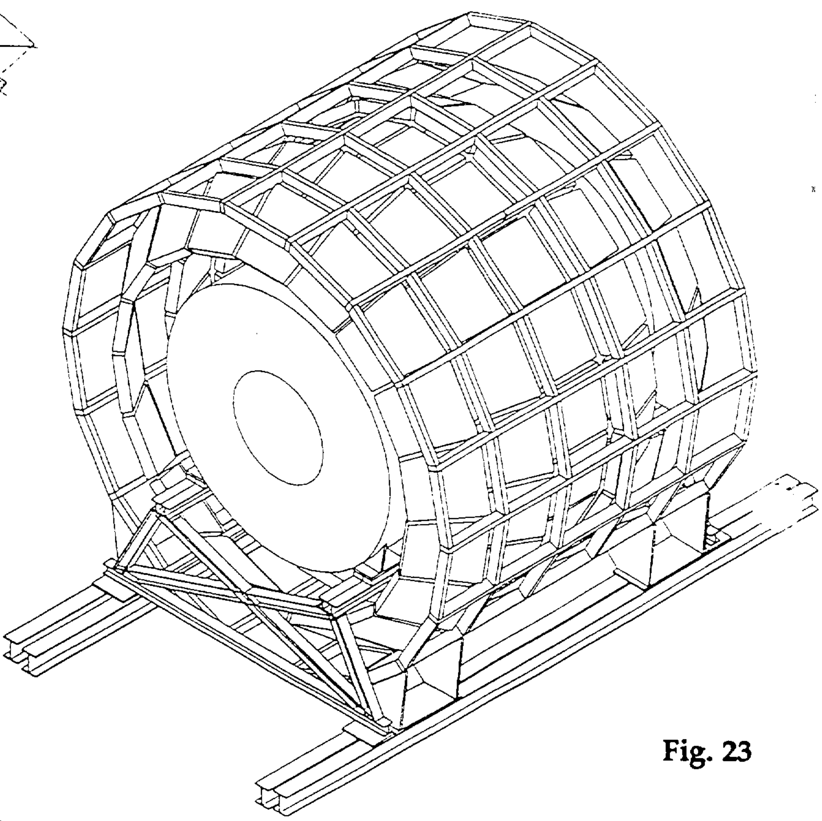
b)

Fig. 23

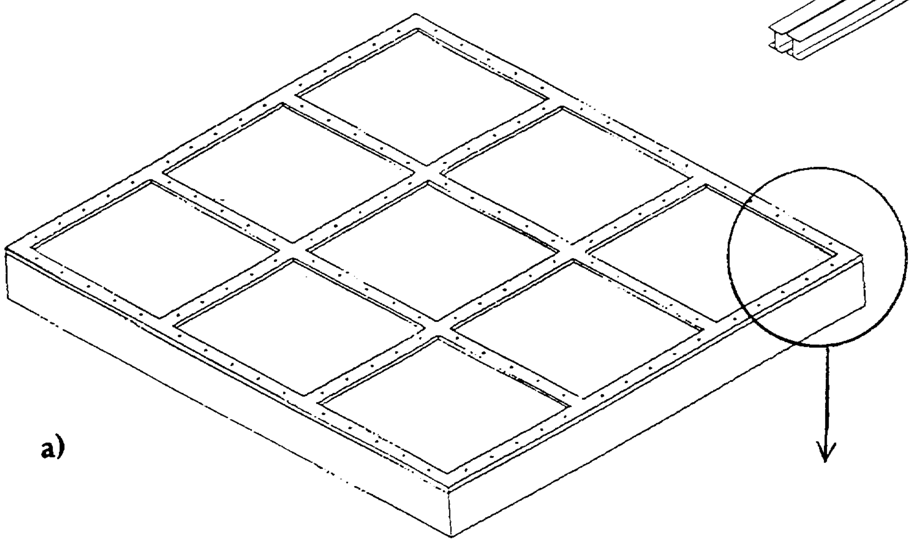
a)

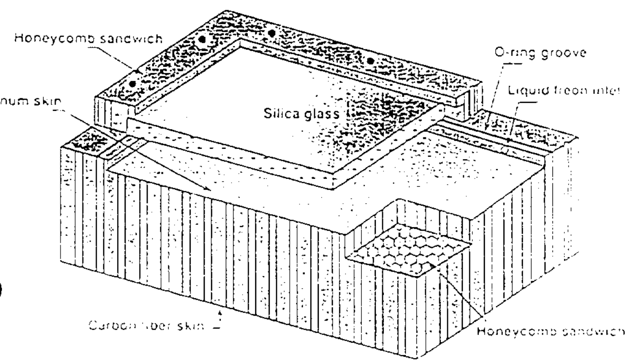
Honeycomb sandwich
O-ring groove
Liquid freon inlet
Alluminum skin
Silica glass
b)
Carbon fiber skin
Honeycomb sandwich

Fig. 24

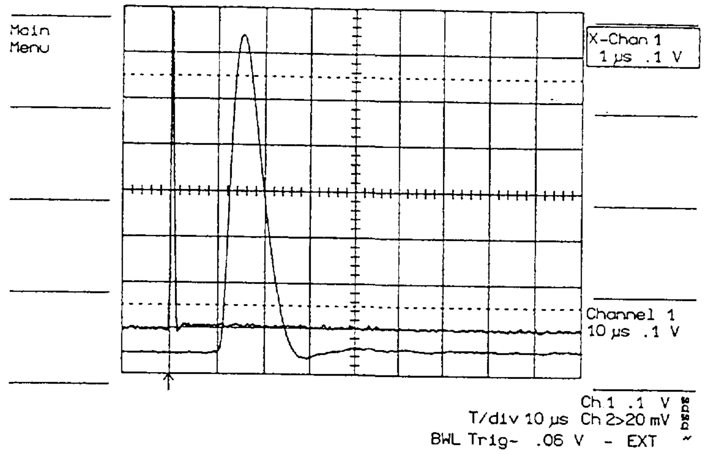

a)

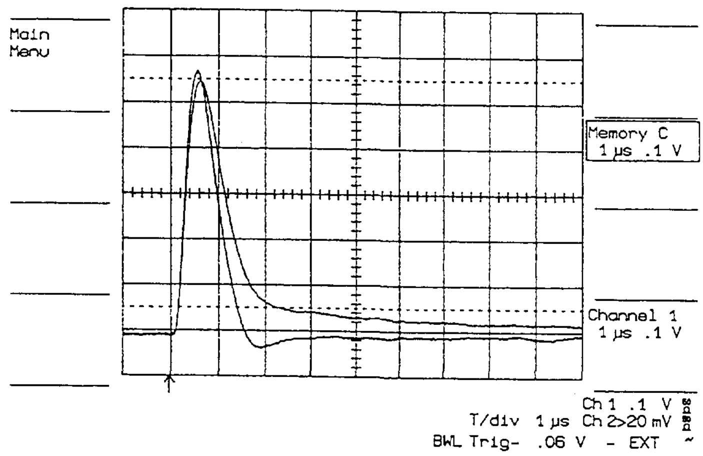

b)

Fig. 25

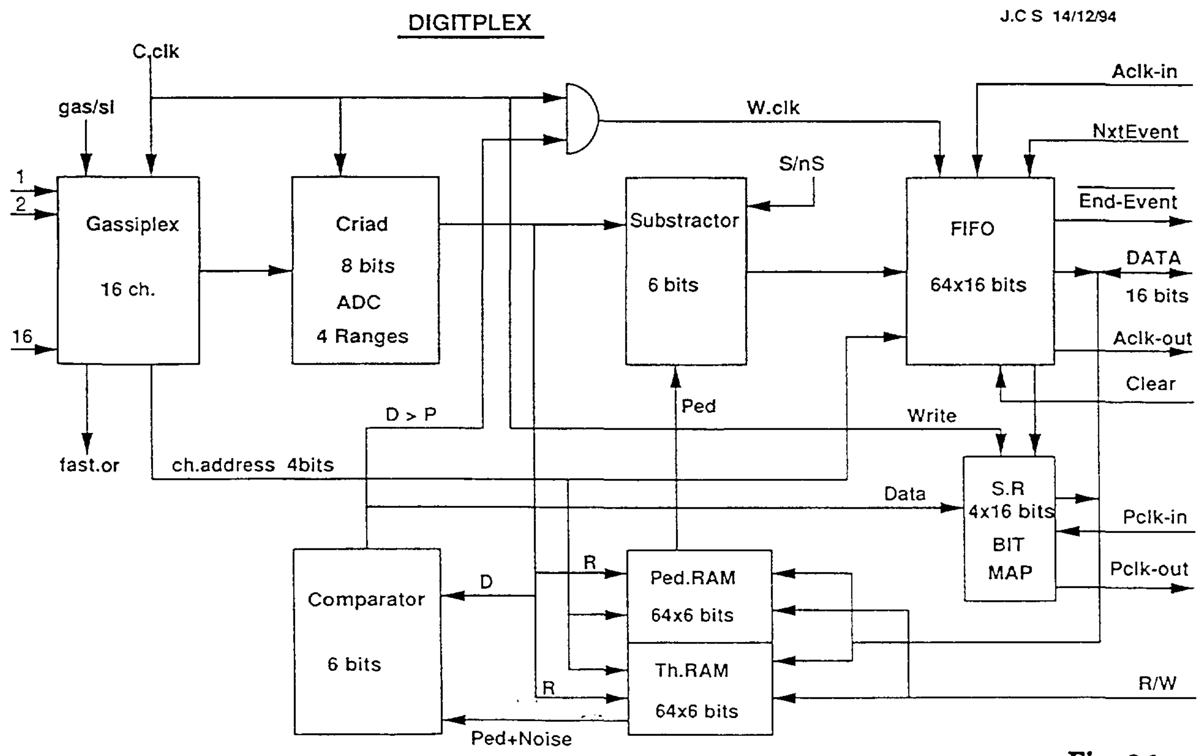

Fig. 26